Pre-normative REsearch for Safe use of Liquid Hydrogen (PRESLHY)

Project Deliverable

Theory and analysis of ignition with specific conditions related to cryogenic hydrogen

Deliverable Number:	24 (D4.1)
Work Package:	4
Version:	1.2
Authors:	Kieran Lyons, Christophe Proust, Donatella Cirrone, Phillip Hooker, Mike Kuznetsov, Simon Coldrick
Submission Date:	28 February 2020
Due Date:	30 June 2019
Report Classification:	Public

This project has received funding from the Fuel Cells and Hydrogen 2 Joint Undertaking under the European Union's Horizon 2020 research and innovation programme under grant agreement No 779613.

Deliverable	
Contractual delivery date	30th June 2019
Actual delivery date (unrevised version)	4th February 2020
Deliverable Number	D4.1
Deliverable Name	Theory and analysis of ignition with specific conditions related to cryogenic hydrogen
Internal document ID	24
Nature	Report

Revisions/Approvals			
	Name	Organisation	Date
WP Leader	Jonathan Hall	HSE SD	04/02/2020
	Jennifer Wen	UWAR	24/02/2020
V1.2 (minor corrections & cover page)	Thomas Jordan	KIT	28/02/2020

Disclaimer

Acknowledgments

This project has received funding from the Fuel Cells and Hydrogen 2 Joint Undertaking under the European Union's Horizon 2020 research and innovation programme under grant agreement No 779613.

Publishable summary

In order to facilitate the use of liquid hydrogen (LH_2) outside of typical industrial applications, for example as a fuel for road vehicles, the understanding of certain high risk scenarios needs development. The PRESLHY project aims to address the most relevant and poorly understood phenomena.

The previous work of this project identified a number of ignition phenomena relevant to LH_2 release scenarios. Based on that review, three knowledge gaps were identified: the influence of low temperature on the flammability limits of hydrogen gas; minimum ignition energy and ignition energies of cryogenic H_2/air mixtures; and electrostatic charging and ignition of multiphase jets.

A brief review of LH_2 release scenarios has been undertaken to inform examination of the relevant theoretical aspects of ignition. Analytical and numerical methods have been developed for the prediction of both minimum ignition energy and hot surface ignition as electrical sparks and hot surfaces are fundamental to many practical ignition scenarios. A number of basic approaches for calculating electrostatic charging in flowing LH_2 have also been presented.

The theoretical work has identified areas for which there remains a lack of detailed experimental data. These are the dependence of minimum ignition energy and hot surface ignition on the initial mixture temperature; the potential process of solid formation and break up of material introducing a charging mechanism; and how the generation of a charge in a flowing stream can be related to the occurrence of an ignition event. A lack of empirical data has also been identified regarding the behaviour and composition of the pool and solid formations following a release of LH_2.

The PRESLHY experimental programme has been designed to provide this information.

Key words

Minimum ignition energy, analytical, numerical, cryogenic, liquid hydrogen, LH_2, electrical spark, electrostatic, multiphase, ignition, lower flammability limit, upper flammability limit, hydrogen/air mixtures.

Abbreviations

AIT	Auto-Ignition Temperature
ASTM	American Society of Testing Materials
BOS	Background Oriented Schlieren
CVD	Chemical Vapour Deposition
FF	Flammability Factor
HSL	Health and Safety Laboratory
HSE	Health and Safety Executive
INERIS	Institut National de l'Environnement Industriel et des Risques
KIT	Karlsruhe Institute of Technology
LFL	Lower Flammability Limit
LH_2	Liquid Hydrogen
MIE	Minimum Ignition Energy
MPE	Minimum Energy Pulse
PDF	Probability Density Function
RPT	Rapid Phase Transition
UFL	Upper Flammability Limit
UU	University of Ulster

Table of Contents

1. Introduction

In order to facilitate the use of liquid hydrogen (LH_2) outside of typical industrial applications, for example as a fuel for road vehicles, the understanding of certain high risk scenarios needs development. The PRESLHY project aims to address the most relevant and poorly understood phenomena.

The state of the art report (2018) [1] compiled as part of this project identified a number of ignition phenomena relevant to LH_2 release scenarios. Based on that review, three knowledge gaps were identified: the influence of low temperature on the flammability limits of hydrogen gas; minimum ignition energy and ignition energies of cryogenic H_2/air mixtures; and electrostatic charging and ignition of multiphase jets.

While there is a significant body of theoretical and practical work on ignition of gaseous hydrogen at ambient temperatures, there is relatively little information relating to ignition of hydrogen at the cryogenic temperatures expected from LH_2 releases. The aim of this report is to:

1) identify ignition fundamentals that underlie practical ignition sources,
2) develop theoretical treatments and to identify further knowledge gaps to be addressed by the PRESLHY experimental programme.

Section two of the report gives a brief review of LH_2 properties including leak sources and their relevance to various ignition phenomena.

Section three covers theoretical aspects of ignition, including analytical and numerical determination of minimum ignition energy for ambient temperature conditions and charge generation resulting from flowing LH_2.

Section four presents conclusions from the work and highlights the areas to be investigated further by the experimental programme in the PRESLHY project.

2. Ignition of cryogenic mixtures

The need to store hydrogen in its liquid state means that releases at cryogenic temperatures are possible. An understanding of the implication and consequences of any likely ignition is therefore required. Table 1 shows the properties of (LH_2), and how these compare to the other components of air.

Table 1 – Properties of cryogenic substances [2]

	Hydrogen	Nitrogen	Oxygen
Liquid Density (kg/m^3)	70.8	804	1142
Gas density at boiling point (kg/m^3)	1.34	4.61	4.48
Boiling point (K)	20.28	77.35	90.18
Freezing point (K)	14.01	63.29	54.75

During a spill of LH_2, differences between typical ambient and storage conditions lead to the potential for hydrogen to exist in multiple physical phases. These phases can also entrain additional condensates (e.g. condensation of water vapour or other lower volatility gases) to form dual-phase mixtures. Potentially, each of these mixtures has different sensitivities and responses to ignition. The experiments described by Jalais *et al* in the state of the art report (2018) [1] showed the behaviour of LH_2 spills and identified common hydrogen mixtures that would be present in the event of an accidental spillage; ignition mechanisms and combustion properties were also comprehensively reviewed. This section includes a summary of the commonly occurring cryogenic mixtures and a brief review of some additional relevant work to aid in the understanding of the related phenomena. A more in-depth review of LH_2 properties and release mechanisms is provided in deliverable D3.1 Theory and Analysis of Cryogenic Hydrogen Release and Dispersion [3].

2.1. Multiphase jets

At the release point of pressurised LH_2 through an orifice, a mixture of gaseous and liquid hydrogen forms due to the flash vaporisation of the cryogenic liquid upon introduction to ambient conditions. The storage pressure and geometry of the release nozzle or hole through which LH_2 passes are significant factors in determining the volume and flow rate of any spill. For example, increasing the pressure difference across a constant orifice will increase the proportion of LH_2 that undergoes flash vaporisation. Cryogenic temperature releases of LH_2 may also result in solid phase material accumulation on, or near, the release point. This solid material may intermittently break off into the flowing stream presenting additional implications for electric charge generation.

Predicting proportion of flash vaporisation in a multiphase, cryogenic jet

An accurate estimation of the vaporised proportion is vital to accurately predict the behaviour of a pressurised release of LH_2. This is due to the vaporised proportion having a large impact on the release velocity and the subsequent behaviour of any hydrogen pool and vapour cloud formed. The proportion of liquid in the dispersing jet may also influence electric charge generation. Giannissi and Venetsanos (2017) [4], detailed that the vaporisation process could be modelled as either isentropic or isenthalpic. When simulating LH_2 release experiments conducted by HSL [2], the opportunity to compare the output of the two models was taken. It was found that the relative difference between the two was 11.35% with a simulated applied storage pressure of 2 bar through a 26.6 mm diameter

hole. The reference further details that the relative difference between isentropic and isenthalpic simulations increased as the pressure (and vapour mass fraction) increased leading to the following conclusion:

"Isenthalpic flashes provide good approximations unless the liquid mass fraction is very small." [4] [5]

Due to these findings, the vapour mass fraction in the model of Giannissi and Venetsanos was calculated from the following equation, which itself was derived from an energy balance equation.

$$q_v = \frac{h_{1L} - h_{2L}}{h_{2V} - h_{2L}} \qquad \textit{(Eq. 1)}$$

Where q_v = the vapour mass fraction,

h_{1L} = the enthalpy of the liquid at storage conditions (J),

h_{2L} = the enthalpy of the liquid at exit conditions (J),

h_{2V} = the enthalpy of the vapour at exit conditions (J).

From these initial conditions Giannissi and Venetsanos went on to model the dispersion of the vapour cloud from the experiments with success, suggesting that the isenthalpic model of flash vaporisation was sound. This model agreed closely with the work of Tao Jin *et al* (2017) [6], while modelling experiments for NASA, they also used a two-phase flow model and isenthalpic expansion, achieving similar results to those of Giannissi and Venetsanos.

Due to the success that the modellers have had with predicting the behaviour of the hydrogen vapour clouds, an isenthalpic model seems sufficient for low pressure LH2 releases, and as such is not a specific point of further investigation. However, the data gathered in the planned experimental campaign will provide further verification for the method.

Observations of cryogenic hydrogen jets

Experiments conducted by Veser *et al* (2011) [7] studied the release of horizontal jets of hydrogen through different nozzle sizes and at different temperatures. Part of the experiments involved studying the movement and profile of unignited jets at cryogenic temperatures. During these trials it was observed that cryogenic releases behaved as typical high momentum jets before becoming buoyant. This is shown in Figure 1 which is a Background Oriented Schlieren (BOS) image of a release of 10 bar hydrogen through a 4 mm diameter hole. In this case, the jet was momentum- driven for approximately 2 m before becoming buoyant.

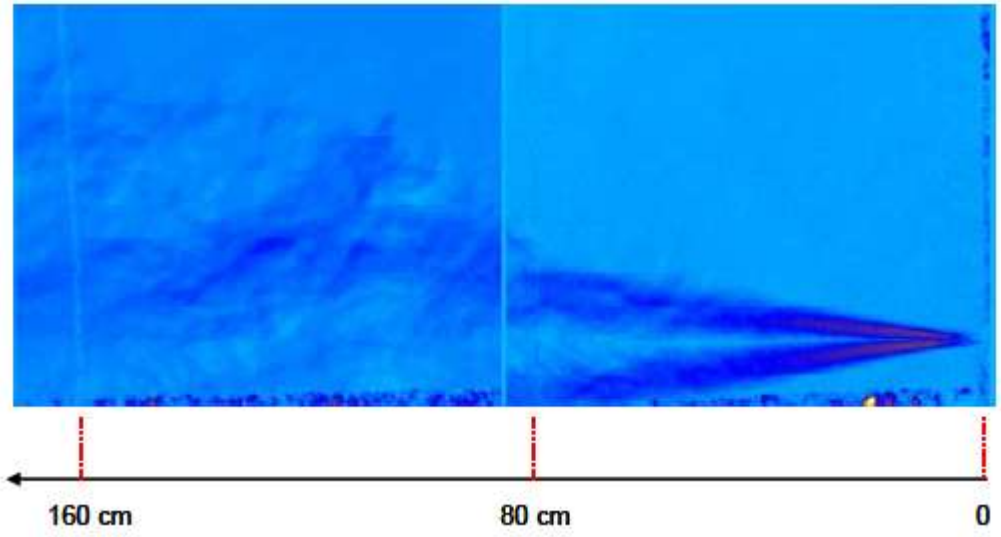

Figure 1 – Background Oriented Schlieren (BOS) image of jet release.

Froude numbers were calculated by Veser for a selection of unignited jets through 1 and 4 mm diameter nozzles at 35, 80 and 300 K. As shown in Figure 2, the calculated Froude numbers are above 1000 even for temperatures as low as 35 K, indicating that the flows are inertia dominated over the temperature and nozzle diameter range studied.

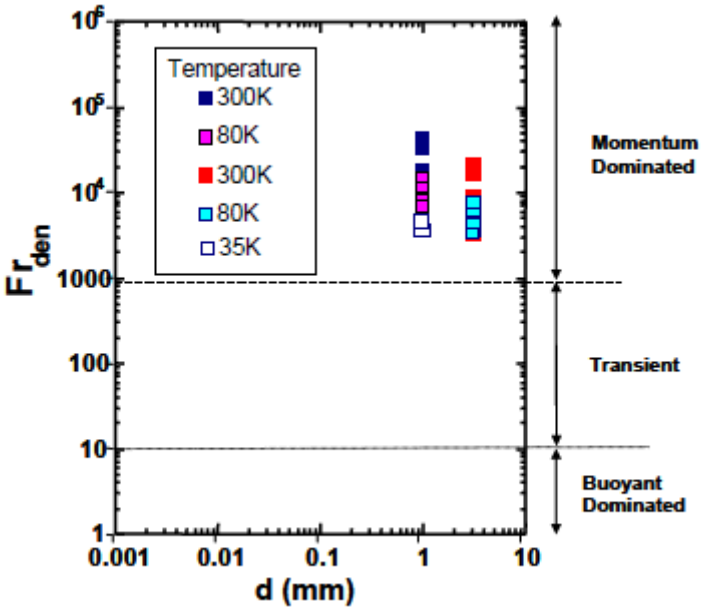

Figure 2 – Froude numbers for a selection of unignited jets with various temperatures and two different nozzle sizes.

Further to calculating the Froude numbers, Veser undertook gas concentration measurements for each trial using 0.3 litre gas probes arranged radially and axially across the jet. The axial distance from the nozzle was then normalised to the nozzle diameter to establish a direct comparison between the hydrogen concentration and the distance from the nozzle including the two different nozzle diameters used. This normalised distance was then multiplied by the square root of the ratio of ambient and hydrogen densities, leading to a positive linear relationship between the inverse of the gas concentration and the

normalised distance parameter. This linear relationship translates to a hyperbolic decay in hydrogen concentration along the centreline of the jet. This relationship held true between 65 and 298 K. However, the results gathered with a temperature of 35 K deviated from this pattern, which was attributed to two phase flow.

While these results show gaseous high pressure hydrogen releases at cryogenic temperatures behave as typical momentum- driven jets, the results at 35 K attributed to dual phase flow are worthy of further investigation. As such, several experiments within this project are planned to address these phenomena.

Quantifying the likelihood of ignition in a gaseous hydrogen jet

Work undertaken by Schefer *et al* (2010) [8] quantified the full extent of the flammable region around a momentum- dominated turbulent hydrogen jet. By using lasers as a non-intrusive measurement and ignition tool, measurement of hydrogen concentration across the jet were taken and ignition was attempted at various points through the turbulent jet.

Both flame propagation and the creation of a stable jet fire were heavily dependent on the location of the ignition. Two distinct regions were identified and the definitions given in the report follow:

"(1) nearest the central part of the jet at moderate downstream distances, the flame kernel resulting from local ignition propagates outward from the ignition point giving rise to the complete light-up of the jet and the formation of a continuous, stable flame."

"(2) radially outward toward the ambient air, the flame kernel and any flame generated is convected downstream where it is eventually extinguished."

The transition from one region to the other was coined as the "*lightup boundary*". Figure 3 shows this boundary in a hydrogen jet, where each point in the boundary is an average of 5 tests.

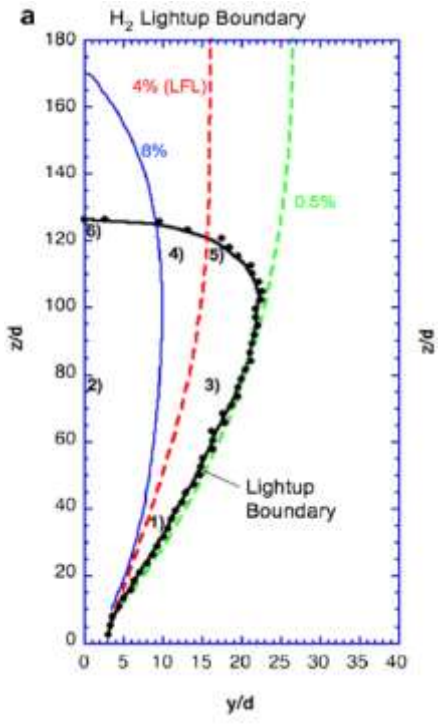

Figure 3 – Lightup boundary in an average hydrogen jet.

The regions were then characterised by a series of inequalities relating to the probability of ignition (P_I), the probability of a jet fire being formed (P_L) and the ratio of axial or radial distance to the diameter of the release point (z/d) or (r/d). These probabilities were established through repeated tests of ambient temperature H_2 jets with an exit velocity of 134 m/s. The probabilities alter with the distance to release diameter ratio as the distance is highly coupled with the gas concentration. By comparing the ratio with gas concentration and the probabilities, it can be concluded that ignition will not occur above the UFL or below the LFL, but flame light up will not occur below 8% concentration H_2. This has been attributed to the static LFL not accounting for turbulence within jet.

Due to the turbulent mixing of the jet, there are fluctuations in the gas concentration at any given point. This means that the average concentration of hydrogen is not an accurate measure to predict the likelihood of ignition as areas of the jet with an average concentration below the LFL could still contain transient ignitable pockets. To reflect this, a term Flammability Factor (FF) is defined as:

"The cumulative probability of finding a flammable mixture at a given point in a turbulent flow."

This parameter was also calculated by Schefer[8] from the experimental results as the fraction of time that the concentration was between the UFL and LFL. The FF was shown to provide a good estimate of the probability of ignition.

A PDF was derived to predict the likelihood of concentrations existing at a given point. Integration of the PDF between the LFL and UFL results in the theoretical FF for the jet. By combining a Gaussian PDF with an intermittency factor, a delta function and a unit step function, Eq. 2 was formed. The intermittency factor, defined as the fraction of time that a point on the flow has a concentration greater than a threshold level and ranges between 0 in the non-turbulent air outside the jet to 1 along the centreline.

$$P_C(f) \equiv (1-\gamma)\delta(\varepsilon)[H(f) - H(f-\varepsilon)] + \gamma P_G(f)[H(f) - H(f-1)] \qquad \textit{(Eq. 2)}$$

Where f = mass fraction of H_2

γ = the intermittency factor

H(f) = 0 for f < 0

H(f) = 1 for f ≥ 0

ε = 0.0025

Due to the step function, the resulting equations are:

$$P_C(f) = \begin{cases} (1-\gamma)\delta(\varepsilon) + \gamma P_G(f) & 0 \le f < 0.0025 \\ \gamma P_G(f) & 0.0025 \le f < 1 \\ 0 & f \ge 1 \end{cases} \qquad \textit{(Eq. 3)}$$

As this shows, the composite PDF is equal to the Gaussian PDF multiplied by the intermittency factor for most gas concentration values. The resulting curve shows good

alignment with the experimental flammability factor and a reasonable estimate for the probability of ignition until large distances from the nozzle, where the estimate becomes conservative. It is postulated that the cause of this divergence lies with the capacity to measure very small ignitions.

Veser *et al* [7] also conducted turbulent jet ignition experiments and obtained similar results, both in terms of identifying the types of ignition (quenched and full light- up) and that the concentration of H_2 required to cause ignition was above the static LFL. Cryogenic temperatures and, in particular, two-phase flow are likely to have implications for the probability of ignition in hydrogen jets. The behaviour of LH_2 jets is a topic that will be investigated within the PRESLHY project.

2.2. Hydrogen vapour clouds formed from LH_2 releases

Beyond the initial release point, a cloud of gaseous hydrogen and air appears as a mist form. This visible aspect of the mist is formed of condensed and/or frozen water vapour and indicates the presence of the cold hydrogen gas. However, one important observation by Zabetakis and Burgess (1961) [9] is that the visible mist is not the extent of the flammable mixture, as ignition can occur away from the cloud.

The cloud is, arguably, the most hazardous aspect of a release of LH_2. This is due to the capacity for the cloud to explode and the damage such an event could cause. The consequences of ignition will be analysed in work package 5 and the dispersion will be studied in work package 3, but there is significant overlap when determining the ignition probability within the cloud as the LFL is determined by the dispersion of the H_2. The effect of low temperatures on the MIE of the cloud is also an area of study.

Heat transfer from the ground to cryogenic hydrogen clouds

In experiments conducted by at NASA by Witcofski and Chirivella (1984) [10] where LH_2 pressurised up to 690 kPa was released through a 15.2 cm pipe, it was observed that the subsequent hydrogen cloud initially remained close to the ground before becoming buoyant and dispersing. This is particularly prevalent during sustained releases where the cooling of the ground underneath the hydrogen release reduces the available heat transfer to the cloud, which in turn retains a higher density for longer. In the experiments with a longer duration (>85 s) the cloud was observed to travel over 100 m at ground level before becoming buoyant.

While studying the dispersion of liquid hydrogen spills in residential areas, Statharas *et al* (2000) [11] demonstrated the huge impact of heat transfer from the ground. Using the ANDREA-HF computational code, dispersion experiments were modelled. These experiments were carried out close to buildings and consisted of six two minute spills of LH_2 with a mass flow rate of approximately 0.4 kg/s. Sensors captured temperature and hydrogen concentration information.

A trial to study the arrival and departure time of the hydrogen cloud at various sensor locations was carried out in the ANDREA-HF model. Since this trial focused on the initial movement of the spill, heat transfer from the ground was neglected within the simulation. The predicted behaviour was shown to be that of a dense gas cloud. Close to the buildings and the ground the model matches the measured concentration levels fairly well, even characterising the complicated back flow close to the buildings that was observed in the

experiments. However, at sensor locations above the ground and away from buildings, the concentration levels were much lower than the experimental values. To compensate for the over prediction of the dense cloud behaviour, the effect of heat conduction from the ground to the hydrogen was added to the model. The parameters of the ground, such as moisture content, were estimated based on a best fit with the experimental results as they were not measured.

The figures below show the predicted LFL (4%) surface 100 seconds after the scenario initiation. The output in Figure 4 excludes heat transfer from the ground within the model, and Figure 5 contains modelled heat transfer.

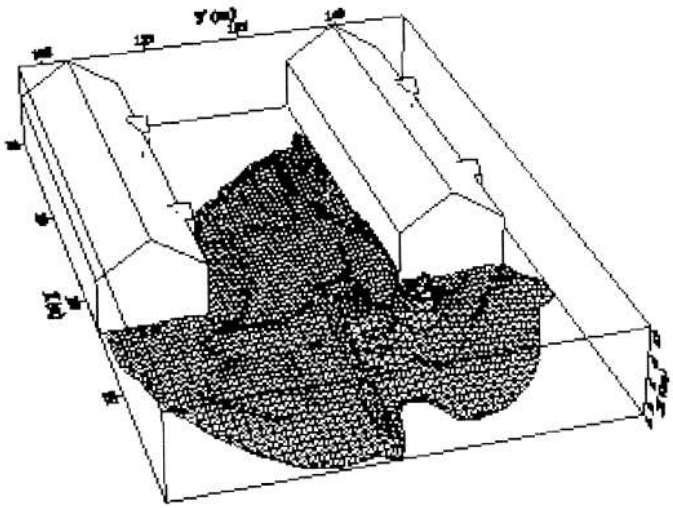

Figure 4 – Output from ANDREA-HF model with no ground heat transfer.

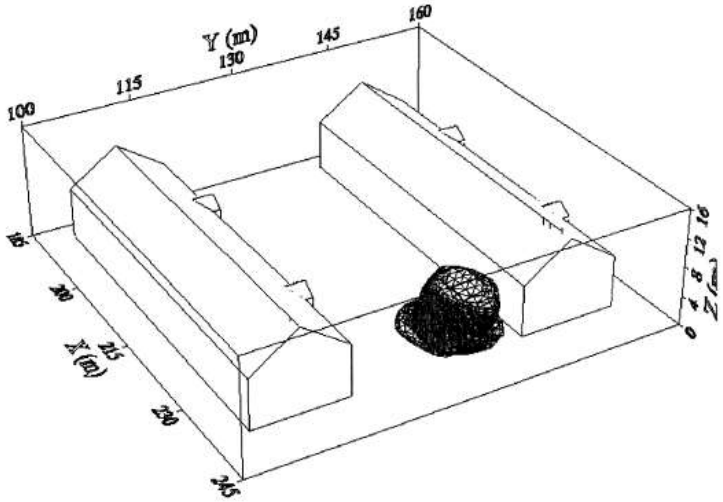

Figure 5 – Output from ANDREA-HF model with ground heat transfer.

The model results indicate that by taking heat transfer into account the flammable region at 100 seconds is much smaller and the dense cloud behaviour is present in a smaller area.

The importance of heat transfer from the ground can be seen to be a pivotal component in the understanding of LH_2 spill behaviour and by extension ignition behaviour.

Effect of temperature of the mixture on flammability limits

The flammability range of a hydrogen-air cloud is affected by the initial temperature of the mixture. The flammability limits for low temperature mixtures were investigated by Wierzba et al. (1992) [12]. The flammability range was determined for upward flame propagation at atmospheric pressure. It was observed that a decrease of temperature from 23°C to -60°C caused a decrease of UFL from 73.5% to 71.2% by vol. This variation corresponds to a reduction by approximately 3% of hydrogen content in air. An increase by approximately 10% was observed for the LFL, which varied from 3.9% to 4.3% when temperature decreased from 23°C to -100°C. The authors compared their experimental results to the LFL and UFL calculated using Burgess-Wheeler correlations (Zabetakis, 1965) [13]:

$$\frac{LFL_T}{LFL_{T_0}} = 1 - 0.000721(T - T_0) \qquad \textit{(Eq. 4)}$$

$$\frac{UFL_T}{UFL_{T_0}} = 1 + 0.000721(T - T_0) \qquad \textit{(Eq. 5)}$$

Where T = temperature of the mixture (°C)

T_0 = reference temperature for which the corresponding value of LFL_{T_0} is available (°C).

The authors found that correlations reproduced experiments with reasonably good accuracy over the considered temperature range. The relative deviation for lean mixtures resulted to be 1.25%, whereas it reached almost 3% for the rich mixtures.

In an experiment with similar focus, Liaw and Chen (2016) **Fehler! Verweisquelle konnte nicht gefunden werden.** used the energy balance equation to determine the LFL and UFL for several fuels, including hydrogen defining a relationship as shown in Eq. 6:

$$\Delta H^0_{298} + \sum_{reactants} \int_{T_i}^{298} n_j cp_j dT + \sum_{products} \int_{298}^{T_f} n_j cp_j dT = Q_r \qquad \textit{(Eq. 6)}$$

Where ΔH^0_{298} = the standard reaction heat at 298 K (J)

n_j = the number of moles heat capacity (J mol^{-1} K^{-1})

cp_j = heat capacity (J mol^{-1} K^{-1})

T_i = temperature of the fresh mixture (K)

T_f = temperature of the burnt mixture (K)

Q_r = heat loss through thermal radiation (J mol^{-1})

A first analysis was conducted assuming adiabatic conditions ($Q_r = 0$). The capability of the model was assessed by comparison against experiments on low temperature hydrogen-air mixtures by Wierzba et al. (1992) [12] and Karim et al. (1984) [14]. The latter investigated the flammability limits for mixtures with temperature down to -130°C. Liaw and Chen

(2016) [15] found an excellent agreement between the UFL measured experimentally for mixtures down to -50°C and their calculations. A good accuracy was found for the prediction of the LFL measured by Karim et al. (1984) [14] for temperature from -130°C to 25°C. A greater deviation was found from the LFL experimentally measured by Wierzba et al. (1992) [12], with a maximum value equal to 0.94%. The reason may be due to the different experimental configuration adopted in Wierzba et al. (1992). It was found that the equation used to calculate the heat capacity did not affect the resulting LFL and UFL values, in contrast to what observed for methane.

A second analysis was conducted including the heat losses by radiation to the environment surrounding the experimental apparatus ($Q_r \neq 0$). It found a negligible effect on the calculated LFL and UFL. The authors justify these results as follow: the time employed by the flame to propagate is too short to heat up the walls of the experimental apparatus to a temperature high enough to initiate a significant heat transfer with the surrounding environment, almost approaching adiabatic conditions.

2.3. Liquid hydrogen pools

Pools of LH_2 are formed in some circumstances, particularly during large, sudden releases of LH_2 and continuous releases close to the ground. In continuous releases the pool is formed by the proportion of LH_2 that does not undergo flash vaporisation. As described by Verfondern and Dienhart (1996) [16], LH_2 pool spreading can be categorised into two parts. In the initial period both the radius of the pool and the rate of vaporisation of the pool increase until a steady state is reached. The steady state is characterised by the equilibrium between the vaporisation and release rates. In the second stage, the radius of the pool continues to grow as the ground cools, reducing the heat transfer per unit area.

In LH_2 spill experiments conducted by Royle and Willoughby at HSL (2012) [17], it was postulated that the pool is highly unlikely to be pure LH_2 but is also likely to contain liquid air. Since the condensing point of oxygen and nitrogen is above the temperature of LH_2 a physical phase change is possible, condensing solid phase components into the pool. Further evidence of this was found in the formation of a solid deposit, thought to be condensed air, which was formed during these spills as shown in Figure 6.

Planned experiments in the PRESLHY project are designed to characterise the proportion of LH_2 that undergoes flash vaporisation during elevated releases. The remaining proportion that remains liquid and falls to the ground, the rainout, has the potential to form pools and the aforementioned condensed phase, although the solid formation appears to be highly condition specific so may not be reproduced.

Figure 6 – Solid deposit formed during unignited HSL experiments.

Interaction between liquid hydrogen and water

There is limited information on the interaction between liquid hydrogen and water. Verfondern and Dienhart [16] conducted an investigation into LH_2 pool spreading, which included large scale hydrogen releases onto a 3.5 m diameter pool of water.

The observed behaviour showed a visible liquid hydrogen pool forming on the surface of the water. The diameter of the hydrogen pool fluctuated over time due to irregularities in the flow and turbulence induced from the release. Following a continued release, a layer of ice formed on the water where the cryogen had been in contact.

Due to the cryogenic temperatures of LH_2, there is the potential for a rapid phase transition (RPT) explosion in the event that liquid water and LH_2 interact. As part of the PRESLHY project, experiments investigating the behaviour of a pool of LH_2 when a sprinkler system or water hose is introduced will be conducted.

3. Theory

3.1. Introduction

Explosion issues are usually addressed under the implicit assumption that ignition is possible. Therefore, working practices are put in place to mitigate against ignition probability and ignition consequences. Asbury and Hawksworth (2007) [18] indicated that even a massive leakage does not automatically ignite but that, when it does, the exact reason for igniting is unknown. The authors discussed a few possible ignition mechanisms and concluded that static electricity resulting from high velocity flow of hydrogen could explain many "spontaneous" ignitions. From this kind of information, a list of practical ignition causes in industry can be obtained (Table 2).

Table 2 – Practical ignition causes in industry and potential relevant physical ignition processes

Practical ignition causes	**Potentially relevant ignition processes**
Electrical devices	Spark, hot surface, autoignition (in boxes)
Electrostatic discharges	Spark
Heating devices	Hot surface, autoignition
Strong light sources	Hot surface
Friction and mechanical impacts	Hot surface, spark
Ultrasound and vibrations	Hot surface
High pressure releases	Diffuse ignition, spark, hot surface

This does not provide additional information about the ignition mechanism. However, four different fundamental ignition processes have been identified so far (Proust, 2019) [19]; these are:

1) Auto ignition (Lewis and von Elbe, 1987) [20] theoretically appearing in homogenously heated volumes (thus leading to a volumetric explosion and not to a propagating flame),
2) spark ignition (Lewis and von Elbe, 1987),
3) hot surface ignition (Carleton et al., 1994) [21] ,and
4) diffusion ignition (Wolanski and Wojcicki, 1973) [22].

In practical ignition causes, such as high-pressure releases, several of the aforementioned fundamental ignition mechanisms may be present and relevant. The shock wave may trigger a diffusion ignition, the flow may convey particles which may create electrostatic charge and a spark or a hot spot when impinging on obstacles if large enough. In Table 2, the potentially relevant fundamental ignition processes are tentatively associated with practical ignition causes.

Hot surface and spark ignitions are associated with many practical ignition sources, which justifies further investigation of these mechanisms in the present project.

Fundamental ignition processes suppose the existence of some relevant ignition parameters. Having this knowledge is however only a part of the ignition risk analysis since a physical link should be made between the fundamental ignition parameters and the practical ignition causes.

This last point is an active field of research and is probably insufficiently developed at this time. Interesting contributions have been delivered recently (for instance: Adler et al., 1993 [23]; Proust et al., 2007 [24]; Simon et al., 2013 [25]; Duan et al., 2015 [26]) but an in depth look at these outcomes falls outside the scope of PRESLHY.

3.2. Spark

The understanding and modelling of electric spark ignition is very challenging because the experimental measurements are difficult and the physics and chemistry of the ignition flame ball are complex. A "spark" could be defined as a punctual and instantaneous deposit of energy. In practice, the deposit is neither punctual nor instantaneous. Electrical deposits (breakdown, arc) or focussed laser beams are used and extremely high temperatures are reached in fractions of a second. The use of traditional chemical laws and thermodynamics to account for the ignition process can be questioned.

3.2.1 Determination of Minimum Ignition Energy

As reported by Kumamoto et al. (2011) [27], spark capacitive discharge is the most common technique[*1] to determine MIE for flammable mixtures in experiments. From a safety point of view, it closely resembles electrostatic discharge associated with ignition hazards (Pratt, 2000) [29].

A significant body of work about the measurement of the Minimum Ignition Energy (MIE) was performed more than 50 years ago by Lewis and von Elbe (1951 [30], 1961 [31]) and Calcote et al. (1952) [32]. Since then, the effort has decreased significantly and there is not much interest in directly measuring MIE. It can be noted that the measurement method for MIE of gases and vapours has not been standardised. Indirect means are now favoured, like the Minimum Ignition Current of the Minimum ignition Curve (Eckhoff, 2002) [33].

Eckhoff, (2010) [34], challenged the way the former data were obtained was questioned and in particular the statistics behind it. Due to the large overlap between the ignition points and no ignition points (Figure 7), the experimentalist used probit laws. The ignition threshold might then represent more of a statistic limit than a true physically meaningful border. This statistical nature may come more from the difficulty to master the spark characteristics than from the flame ball development although a complicated flow is produced in the spark which may disturb the flame. For instance, for hydrogen air mixtures, Kumamoto et al. (2011) and Kuchta (1986) [35] in comparing their MIE measurements with Lewis and von Elbe and Calcote observed up to a factor of two difference for lean mixtures.

Ono et al. (2007) [36] demonstrated the influence of gap distance for needle to needle electrodes in hydrogen-air mixtures. It was observed that for a stoichiometric hydrogen-air mixture, MIE decreases with the shortening of distance between the electrodes, until a minimum is reached for 0.5 mm. A further decrease in gap distance caused an increase of MIE, highlighting that not enough mixture is excited by the spark and there is a greater contribution of losses to the electrodes.

[*1] Other techniques have been utilised such as focussed pulsed laser beams (Weinrotter et al., 2005) [28]. In pulsed laser systems, the energy of the pulse is known but not the quantity absorbed by the target gas from the plasma created at the local point. The major part of it has been transmitted through the plasma and dissipated by absorption in other parts of the beam. Because of this, the MPE generally appears on order of magnitude larger than the traditional MIE.

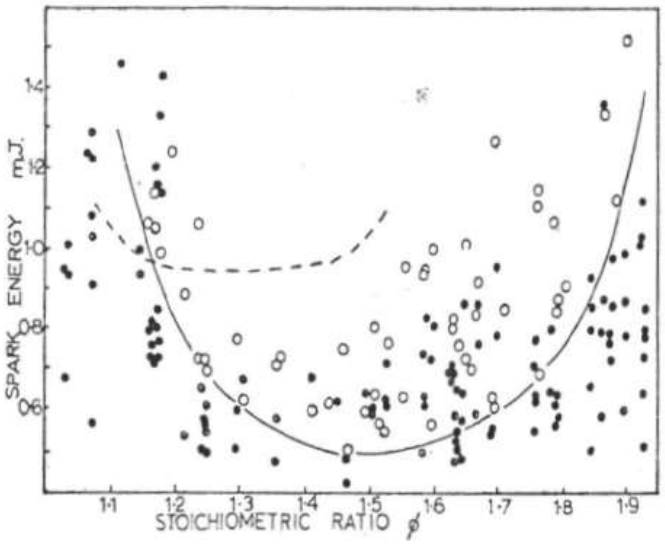

Figure 7 – Illustration of the data scattering about the minimum ignition energy of propane-air mixtures at ambient conditions. (from Eckhoff)

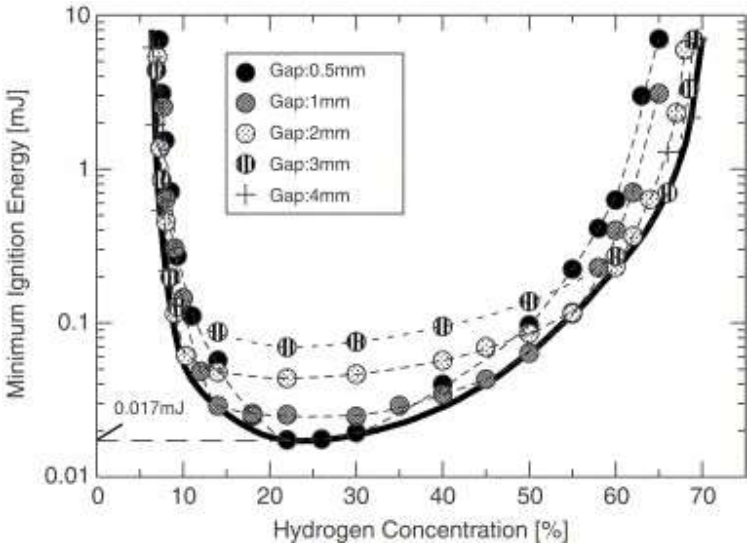

Figure 8 – "Best" measurements of the MIE for hydrogen-air mixtures in standard conditions. (Ono et al. 2007)

Bearing this in mind, the standard MIE of a hydrogen-air mixture (standard conditions) is reported as 0.017 mJ [37] in proximity of a stoichiometric composition (Figure 8). Other flammable gases, such as methane or ethane, are usually characterised by MIE greater than 0.1 mJ (Lewis and Von Elbe, 1961) [31].

The ignition energy depends strongly on the oxygen content in the mixture. This parameter rises in significance in the case of LH_2 or cryogenic releases, where a local enrichment of oxygen can be reached due to the low temperature of the mixture. Kumamoto et al. (2011) [27] measured a decrease of MIE to 0.0057 mJ for air containing 35% by vol. of oxygen. The experimentalists could not measure the corresponding value for hydrogen combustion in oxygen due to a limitation of their experimental apparatus. Kuchta (1986) [35] reported that it can be as low as 0.0012 mJ.

3.2.2 Analytical description of the Minimum Ignition Energy

Authoritative monographs that include ignition processes have been published over the last 50 years regarding the underlying physical mechanisms of flame development (Lewis and von Elbe, 1987 [20]; Glasmann, 1977 [38]; Williams, 1985 [39]; Hattwig and Steen, 2004 [40]). In particular, the classical "thermal explosion theory" described by Hattwig and Steen, (2004) can be used to describe the phenomenology and show the links between ignition and combustion parameters. Comparison of the content of the reports suggest that most analytical developments rely on a highly simplified chemistry and, often, the heat release is represented by a one-step chemical reaction following a global Arrhenius reaction rate such as :

F (fuel) + O (oxidant as air) » P (products) + heat

With the volumetric heat release rate, Q_{comb} (W/m^3, in a simple form):

$$\dot{Q}_{comb} = \rho\, \Delta H_{comb}\, A\, e^{-\frac{E_{act}}{RT}} \qquad \textit{(Eq. 7)}$$

Where: ΔH_{comb} = specific heat release rate per unit mass of the mixture (J/kg)
ρ = density of the mixture (kg/m^3)
A = pre-exponential factor of the Arrhenius law (s^{-1})
E_{act} = activation energy of the reaction (J/mole)
R = universal gas constant (8.314 J/mole/K)
T = temperature (K)

ΔH_{comb} is a property of the mixture and is related to the maximum temperature of the combustion (T_{ad}) as measured in an adiabatic system. If T_0 is the initial temperature, ρ_0 the initial specific mass and Cp the specific heat capacity then Eq. 7 reads:

$$\dot{Q}_{comb} = \rho_0\, A(T_{ad} - T_0)\frac{T_0}{T}\, e^{-\frac{E_{act}}{RT}} \qquad \textit{(Eq. 8)}$$

Because E_{act}/R is typically on the order of 10000 K for most fuel-air mixtures, the evolution of Eq. 8 with T is largely dominated by the exponential term as shown on Figure 7. Note also that this equation is valid for T smaller or equal to T_{ad}. This expression does not include any limitation so that it may be inferred that combustion would occur at any temperature even without any ignition source. The speed of the combustion process would only depend on T. This might be true only if the process was perfectly adiabatic but not when heat losses are taken into account. Unless T is very large, gases exchange heat mainly by convection. Assuming a volume V (m^3) of the gas having a typical size D (in m, for instance $D = V^{1/3}$), then the volumetric heat lost by convection with the surrounding (Q_{comb} in W/m^3) through the external area $A_{exchange}$ (m^2) of V reads:

$$\dot{Q}_{losses} = h_{conv}\frac{A_{exchange}}{V}(T - T_0) \approx h_{conv}\frac{1}{D}(T - T_0) \qquad \textit{(Eq. 9)}$$

where h_{conv} is the exchange rate coefficient (unit of W/m^{2}K), usually approximately constant for a given geometrical configuration and flowing conditions.

It appears that, for a given size D, Eq. 9 varies linearly with T as shown on Figure 7. Equations Eq. 8 and Eq. 9 then describe the behaviour of a pocket of reactant raised at a given temperature T. Suppose a homogeneous and quiescent explosive atmosphere is prepared in a volume V and T is gradually increased. The combustion is active, but initially proceeds extremely slowly. Whilst the heat losses (volumetric rate in W/m^3) are larger than the heat released by the combustion ($Q_{losses} > Q_{comb}$), the chemical reaction is dampened because T is forced to decrease. Because of the exponential temperature dependency of the reaction of combustion, there is a temperature where the heat released by the combustion becomes larger than the linear heat losses ($Q_{losses} < Q_{comb}$). Above this temperature thermal runaway of the reaction and combustion occurs (T increases up to T_{ad}).

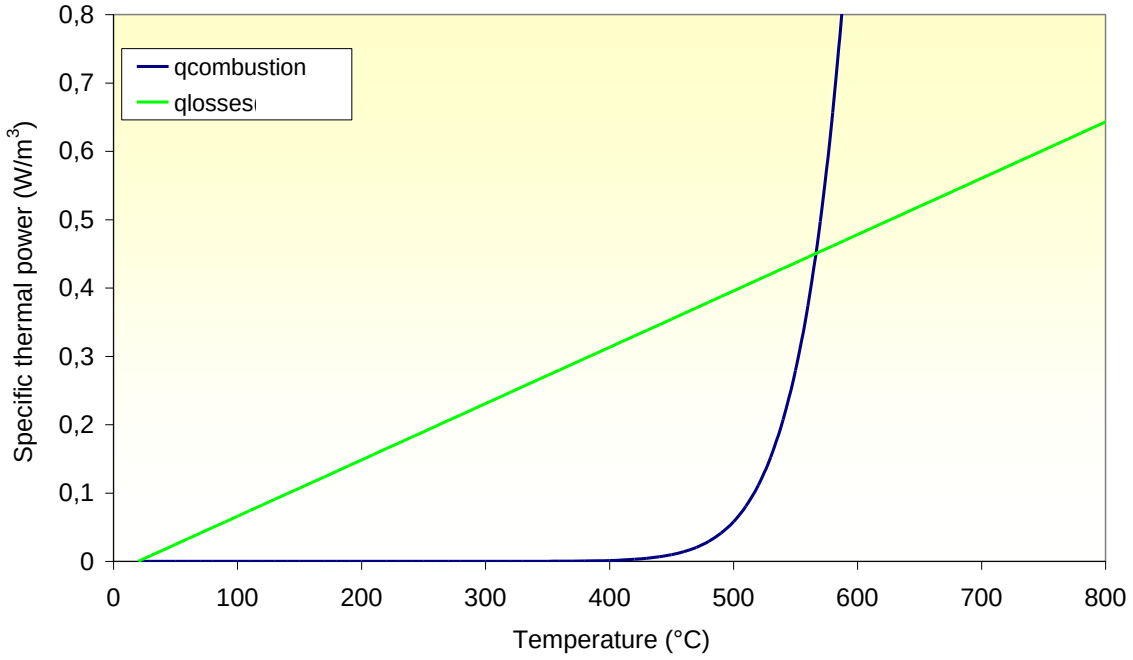

Figure 9 – Volumetric heat release rate and losses in a volume V (featuring the ASTM flash for autoignition temperature measurements) containing a homogeneous and quiescent stoichiometric hydrogen air mixture.

Although it is an over-simplified theory, it is useful to investigate the various possible ignition modes (Carleton and Weinberg, 1994) [41]. A well-known application, particularly fitted to this modelling concept, is autoignition. The autoignition temperature of hydrogen-air mixtures is about 550°C, measured by a 50 mm size flash. The temperature of the flash is progressively increased until the volumetric ignition. The latter occurs when the heat loss curve is tangent to the heat release curve[*2]. This theory was applied in the present work to fit the combustion parameters (A and E_{act}/R). A good agreement (Figure 10) is obtained with A= 10^{10} W/m^3 and E_{act}/R=10000 K. Note this value for E_{act}/R is that recommended for hydrogen air mixtures (Coffee et al., 1983) [42].

[*2] Standard natural heat convection laws are used in Eq. 9.

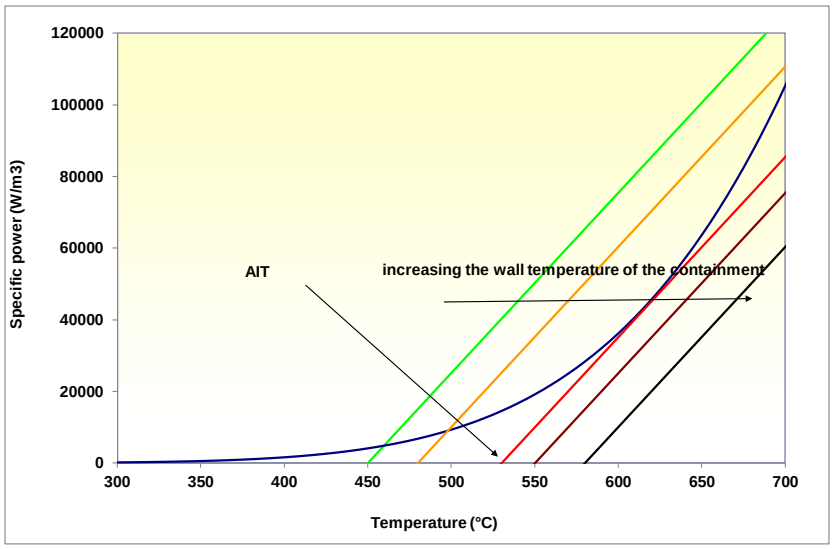

Figure 10 – Fitting of the combustion parameters to retrieve the autoignition temperature of hydrogen-air mixtures.

This modelling approach is now tentatively applied to electric spark ignition mechanisms.

In the spark gap, the heat of the ignition source, E_{spark} (J), is delivered punctually and instantaneously. At this point, D=0 and T is approximated to infinity, so that heat losses are infinite and combustion cannot start. Some (small) amount of time is required for this initial point to spread out due to thermal conduction. Following this initial amount of heat is spread by thermal conduction in the surrounding area but conserved if other thermal losses are ignored (heat radiation, thermal conduction to solid bodies). Throughout this spreading process, the spark energy is conserved according to the following expression (where D increases with time and Cp is the specific heat of the mixture in J/kgK):

$$E_{spark} = \rho_0 \, C_p \, \frac{\pi}{6} \, D^3 (T - T_0) \qquad \textit{(Eq. 10)}$$

The heat loss curve formulated by Eq. 9 (with $h_{conv} \sim 2.\lambda$ where λ is the thermal conductivity of the mixture at the spark temperature so approximately 0.1 W/mK) can now be computed using equation Eq. 10. For each spark kernel size, a temperature is calculated and a specific heat loss. This evolution is presented in Figure 11 for various spark energies (curves labelled “spark”).

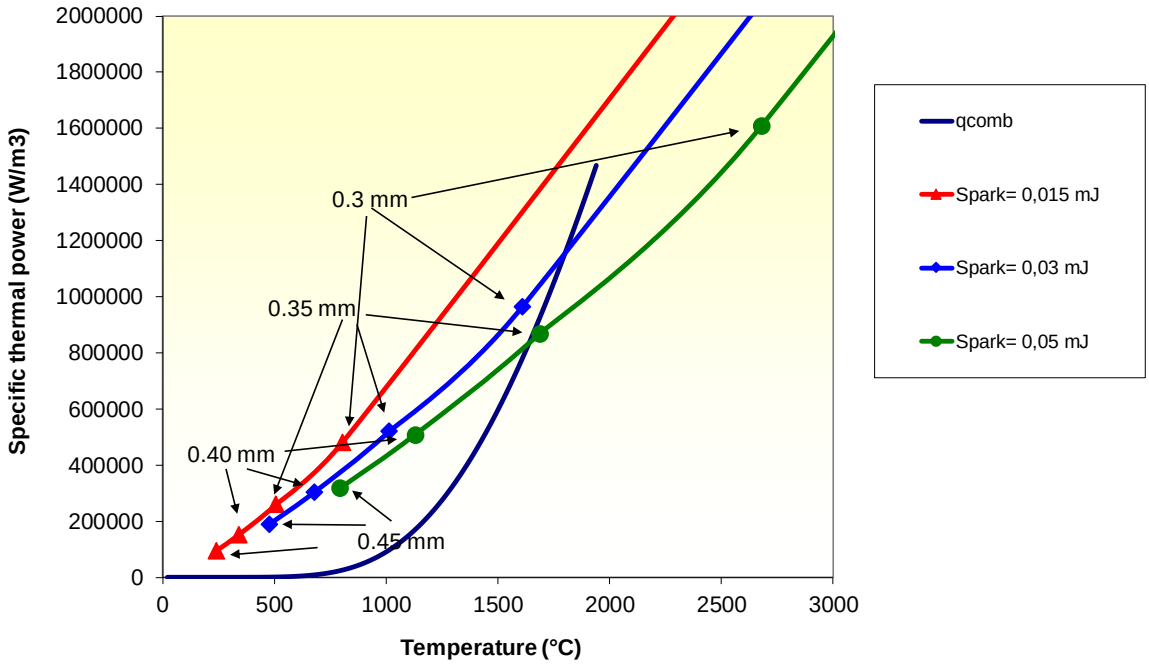

Figure 11 – Simulated spark ignition of a hydrogen-air stoichiometric mixture for three different values of the initial spark energy (arrows and text refer to the hot pocket of gas size at different times)

The heat release represented by Eq. 8 can now be plotted using the values of E_{act}/R and A found as shown in Figure 10. This curve stops at $T=T_{ad}$ with is the maximum combustion temperature. When E_{spark} is too small (E_{spark}=0.015 mJ), the spark heat loss curve (line+triangles) never intercepts the heat release curve and, for any value of T, $Q_{losses}(T)>Q_{comb}(T)$ and the explosion cannot occur. When E_{spark} is sufficiently large (E_{spark}=0.05 mJ), the spark heat loss curve (line+circles) intercepts the heat release curve and the explosion can occur since there is a domain where $Q_{losses}(T)<Q_{comb}(T)$ while $T<T_{ad}$.

The MIE is thus obtained when the intercept is obtained for $T=T_{ad}$, corresponding to the upper point of the heat release curve. This particular point corresponds to a specific size of the hot pocket of gas called the minimum flame kernel, D_{crit}, which is then an intrinsic property of the mixture. It is the minimum size of a flame able to develop in a cold environment. This definition is very close to that of the minimum quenching distance[*3] (D_{quench}). Physically, both parameters can only be proportional.

The main outcomes from this simplified theory are:

- In the MIE conditions, the temperature of the spark kernel is equal to T_{ad} so that Eq. 10 can be used to calculate the MIE;
- T_{ad}, D_{crit} (D_{quench}) and MIE are interlinked. To find the relationship, Eq. 8 and 9 must be equated for $T=T_{ad}$ and $D=D_{crit}\sim D_{quench}$. ($T_{ad}-T_0$) should be replaced by a parameter proportional to E_{spark}/D^3 from Eq. 10. So the heat loss parameter is proportional to E_{spark}/D^4. The heat release parameter at T_{ad}, from Eq. 8 is proportional to the square of the laminar burning velocity S_{lad} of the mixture

[*3] The minimum quenching distance is the smallest gap between two cold parallel planes just allowing the flame to propagate steadily. If the distance is infinitesimally smaller, the flame is quenched.

(Glasmann, 1977) [38]. It is known (Hattwig and Steen, 2004) [40] that D_{quench} and the Sl_{ad} are linked :

$$Pe = \frac{Sl_{ad}\, D_{quench}}{a_{diff}} \approx 50 \qquad \textit{(Eq. 11)}$$

where a_{diff} is the thermal diffusivity of the (cold) mixture (typically 2.10^{-5} m^2/s). So, the heat release parameter is proportional to $1/D^2$. So the MIE should be proportional to the square of $D_{crit} \sim D_{quench}$.

This relationship was discussed Lewis and von Elbe (1961) and this last conclusion is fully confirmed by available data (Figure 12). MIE is approximately proportional to the square of D_{quench}. On this graph, for hydrogen-air mixtures at ambient conditions, MIE=0.017 mJ and D_{quench}=0.7 mm.

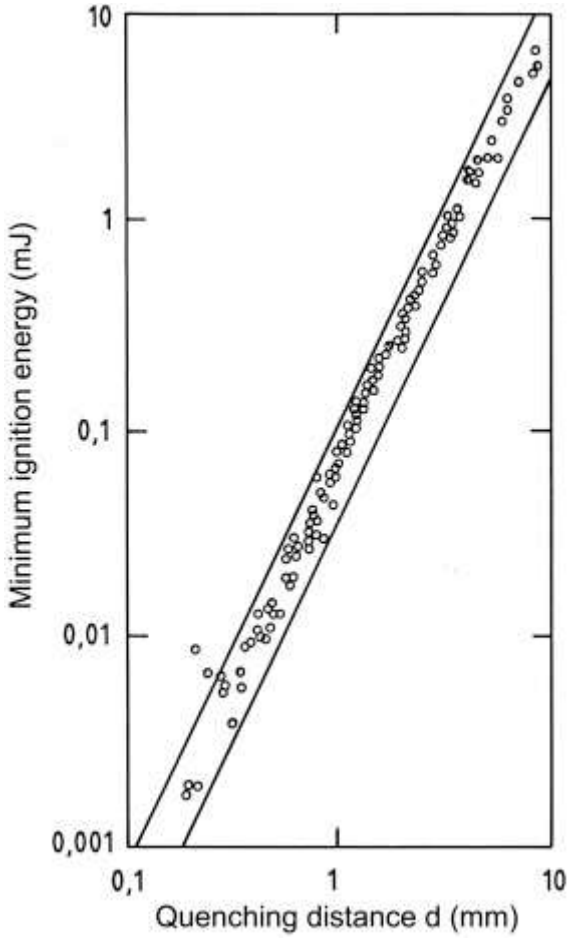

Figure 12 – Relationship between MIE and D_{quench} (from Kuchta, 1985) [43]

A quantitative theoretical estimation is attempted hereafter using the Lewis and von Elbe approach (1961) [31] re-developed by Kondo et al. (2003) [44]. In line with the development above, a first correlation is based on considering the MIE (Eq. 12) as the energy needed to heat up a minimum sphere of the mixture at initial temperature T_i to that of the flame, T_b.

$$MIE = \frac{1}{6}\pi d^3 \rho_b C_{av}(T_b - T_i) \quad \textit{(Eq. 12)}$$

Where ρ_b is the density of the burnt mixture and C_{av} is the heat capacity averaged between the fresh and burnt mixtures. A second equation (Eq. 13) is proposed linking *d* and MIE in a different way, based on the assumption that this amount of energy is just enough to compensate for the heat losses during the ignition delay:

$$MIE = \pi d^2 \lambda_{av} (T_b - T_i) S_{av} \quad \textit{(Eq. 13)}$$

Where λ_{av} and S_{av} are the average heat conductivity and flame speed respectively. Normally the simultaneous resolution of Eq. 12 and 13 should provide MIE and *d*. But it was not used that way by Kondo [44]. This author admitted that *d* was equal to the quenching distance (which is arguable) and used the available experimental data for d=D_{quench}. He included in his work accurate estimates of λ_{av}, S_{av}, C_{av} C_{av}. Under these assumptions, Kondo found that Eq. 13 was more satisfactory, resulting in a MIE approximately twice the experimental measurements for stoichiometric mixtures. UU used both equations to calculate the ignition energy for warm mixtures with hydrogen concentration in air within the range 11-50% by vol. Properties for the fresh and burnt mixtures were calculated through Cantera v2.4.0 [45]. Flame speed in Eq. 13 was calculated using the data on laminar flame speed presented in Lamourex et al. (2002) [46]. Experimental data by Kim et al. (2001) [47] were used for the quenching distance. Results are compared to experimental measurements of MIE in hydrogen-air mixtures by Ono et al. (2007) [36] and Lewis & von Elbe (1961) [31] in Figure 13. Results from Eq. 12 predict the MIE for stoichiometric and fuel rich mixtures well. Prediction worsened for lean mixtures, possibly due to a less accurate determination of the quenching distance in experiments. Eq. 13 resulted in a lower calculated ignition energy, suggesting that the energy needed to compensate the heat losses is lower than the energy required to heat up the fresh mixture to the flame temperature.

This corroborates the chosen modelling approach and the potential dependency with the initial temperature can be discussed.

The dependency of MIE with temperature should largely be found in the variations of D_{quench}, and thus of S_{lad} (and a_{diff}). The laminar burning velocity (Hattwig and Steen, 2004 [40]; Konnov A., 2008 [48]) increases sharply with the temperature (approximately to the square of the absolute temperature). The thermal diffusivity increases almost linearly with the absolute temperature. All in all, D_{quench} should decrease linearly when the temperature increases increase. Consequently, MIE should vary as the square of T_0. This point seems confirmed (Brokaw and Gerstein, 1957) [49] but for higher than ambient temperatures. This has still to be confirmed for lower than ambient temperatures.

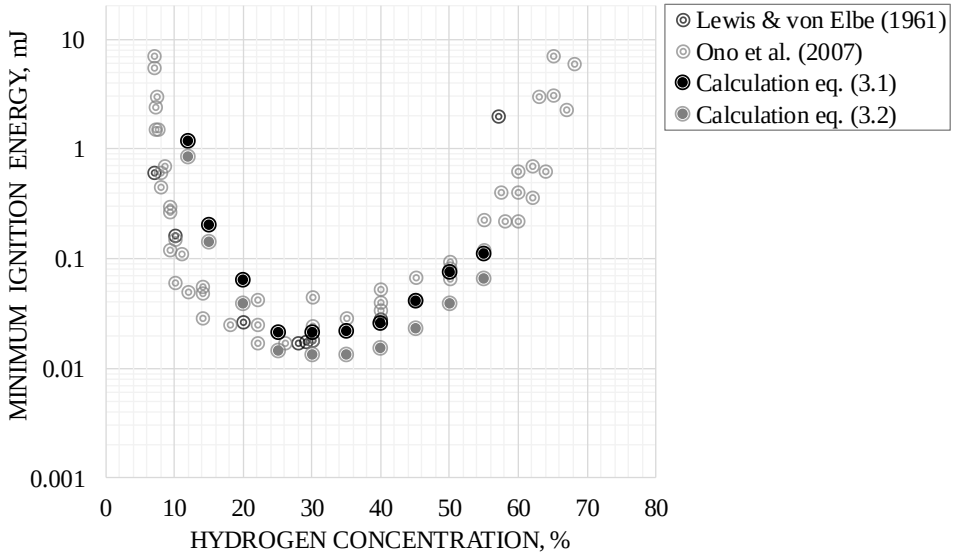

Figure 13 – Comparison of calculated MIE against experiments.

Despite the reasonable agreement achieved with experiments, the theoretical correlations employed experimental data for d and S_u which are currently available only for mixtures at room temperature. Further research should be conducted to include calculation of parameters for cryogenic mixtures, either using software as Cantera (2019) or refining further the theoretical considerations. In addition, there is a lack of extensive experimental data on MIE and S_u for cryogenic mixtures, which are essential for a deeper understanding of the ignition process and validation of analytical and numerical models. These knowledge gaps are being addressed by PRESLHY experimental programme.

3.2.3 Numerical simulations of the Minimum Ignition Energy of hydrogen-air mixtures

Numerical modelling of spark ignition is not straightforward. One of the pioneering works was performed by Wartnatz's team (Mass et al., 1988) [50]. Limited work is devoted to this aspect (Bane, 2010) [51].

Han et al. (2011)[52] found in numerical simulations that the electrode size modelled affected the estimated MIE for gap lengths below the quenching distance. However, the calculated MIE for a stoichiometric hydrogen-air mixture overestimated by over 135% the experimental measurement.

CFD simulations of numerical determination of MIE in hydrogen-air mixtures were conducted by UU to give insights into the spark kernel formation process. The channel radius was considered equal to 60 μm, whereas the electrode radius was assumed to be 0.5 mm, the same as the rods employed in experiments by Ono et al., (2007) [36]. Results agree well with experiments by both Ono et al. (2007) and Lewis & von Elbe (1961), as shown in Figure 14. The heat losses to the electrodes were investigated by analysing two limiting configurations with and without inclusion of the electrodes in the domain. It was found that the presence of the electrodes had a limited effect on the ignition energy for a stoichiometric composition when considering a channel radius and spark gap distance equal to 60 μm and 0.5 mm respectively. The latter is approximately equal to the corresponding quenching distance (Kim et al., 2001) [47]. The MIE resulted to be 9 μJ (one half of the experimental MIE) for both configurations, whereas ignition failed for IE=5.7 μJ. On the other hand, ignition energy was greatly affected for different

concentrations of hydrogen in air and spark gap equal to 0.5 mm. For a mixture containing 10 vol% of H_2 in air, the energy resulting into ignition changed by over one order of magnitude when shifting from one configuration to the other one. No variation was observed instead for a spark gap equal to 2 mm. In this case MIE was determined to be 30 μJ for both configurations (one half of the experimental MIE). In this case, the spark gap is approximately the same as the quenching distance for 10% H_2 concentration (Kim et al., 2001). Therefore, CFD simulation results align with conclusions by Han et al. (2011) on the effect of the electrode size for spark gaps below the quenching distances, although providing a better prediction of the required ignition energy for the range of concentration 10-55%.

The release of energy in a short time (spark duration is assumed to be 1 μs) causes a steep increase of temperature in the spark channel to values that could reach 10000 K (Terao, 2007) [53]. At these temperatures, significant radiation losses may occur. UU conducted a CFD study to analyse their effect, comparing two cases with and without radiation modelling. The gas in the spark channel was assumed to have emissivity equal to 1, given that the high temperature plasma can be treated as a black body radiation source (Science Direct, 2019) [54]. It was showed that radiation losses affect significantly the maximum temperature reached in the spark channel. A temperature of approximately 9000 K was achieved for an energy release equal to 30 μJ, in agreement with analysis by Terao (2007) [53]. However, the MIE for the 10% H_2 mixture was not affected by the inclusion of radiation modelling. The MIE was calculated by gradually decreasing the energy released in the spark channel. The energy discharge leading to ignition was 30 μJ and the energy failing to ignite the mixture was 20 μJ. A more gradual decrease in the energy discharge in simulations, e.g. Δenergy = 5 μJ, may lead to a more accurate determination of MIE and a noticeable effect of radiation losses.

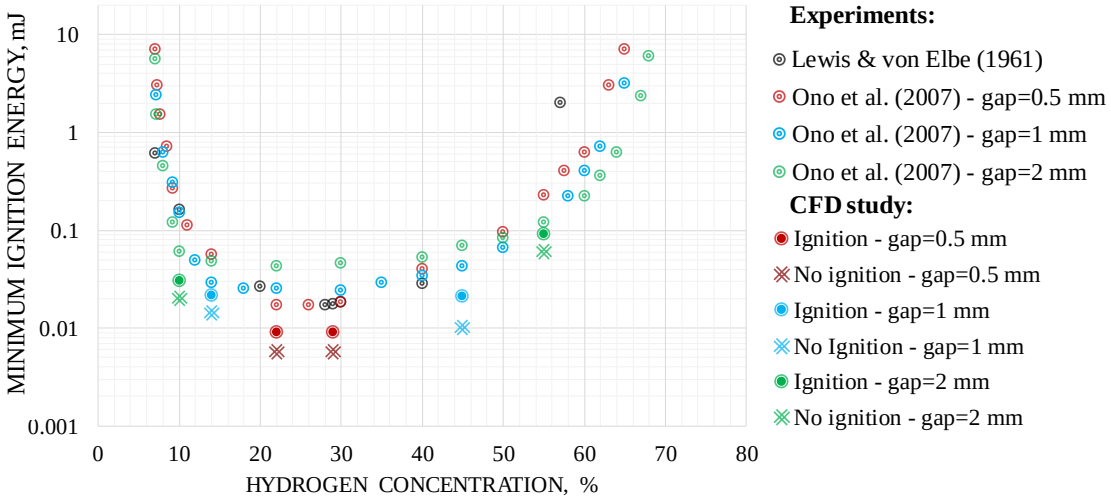

Figure 14 – Comparison of CFD calculations of MIE in hydrogen-air mixture against experiments by Ono et al. (2007) and Lewis & von Elbe (1961).

3.3. Hot surface ignition of hydrogen-air mixtures

Hot surface ignition can occur when a hot surface is placed in a cold flammable atmosphere (cold meaning at a temperature well below the autoignition temperature). If the surface is hot enough, the mixture is ignited and a flame propagates throughout the atmosphere. The minimum temperature at which the ignition is triggered is T_{pcrit}.

3.3.1 Experimental data

The configuration described above has been studied experimentally for nearly one century (Silver, 1937 [55]; Laurendeau, 1982 [56]; Adler, 1993 [23], Powell, 1969 [57]) but only limited data for hydrogen air mixtures is available (Kumar, 1995 [58]; Beyer and Markus, 2012 [59]; Roth et al., 2017 [60]; Buckel and Chandra; 1996 [61], Mevel et al., 2019 [62]).

The influence of the size of the ignition source was identified. When the latter is larger than about the quenching distance (>0.5 mm), the critical hot surface temperature (minimum temperature leading to the ignition) does not depend on the size of the hot surface. Nevertheless, the value of this critical temperature is subject to some debate, varying between 930 and 1100 K in quiescent conditions depending on the data source (Figure 15).

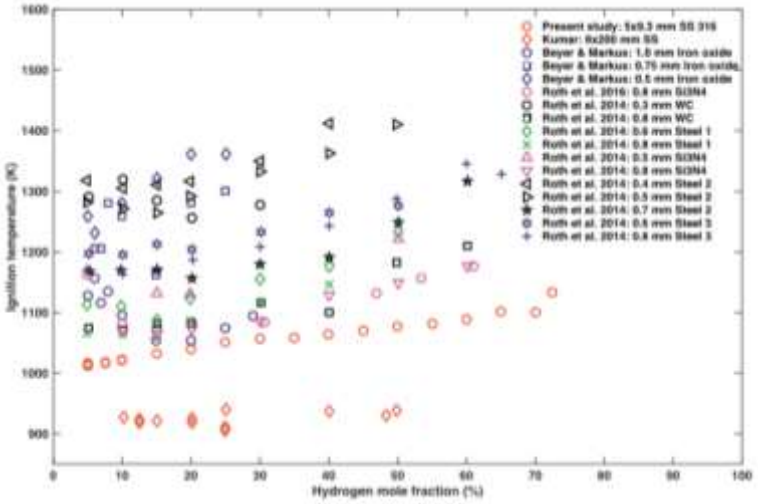

Figure 15 – Variability of the hot surface ignition temperature for atmospheric quiescent hydrogen-air mixtures at room temperature (extracted from Mevel et al., 2019)

To the knowledge of the present author, only Kumar investigated the influence of the "preconditioning" of the atmosphere (pressure, temperature, velocity…). He did that in the specific context of nuclear safety and targeted the influence of the pressure and inerting. Nothing is said about the potential influence of the initial temperature.

3.3.2 Theoretical approaches

Again, self-ignition theory can be used to address this ignition mechanism (Adler, 1993) [23]. Eq. 7 and 8 can be used along with the combustion parameters given in section 3.2.2. The convection coefficients from the literature can again be used. V, the volume of the heated gas pocket, can be viewed as the thermal layer in contact with the hot surface. The thickness of the layer (here the parameter D) is typically comparable to the size of the heated body). The same criteria that for establishing the auto ignition temperature can be used, establishing graphs similar to that of Figure 10 but for different values of D. An example is shown on Figure 16 for D=10 mm. The critical ignition temperature (T_{pcrit}) for hydrogen is about 700°C which is not unreasonable given the available experimental measurements.

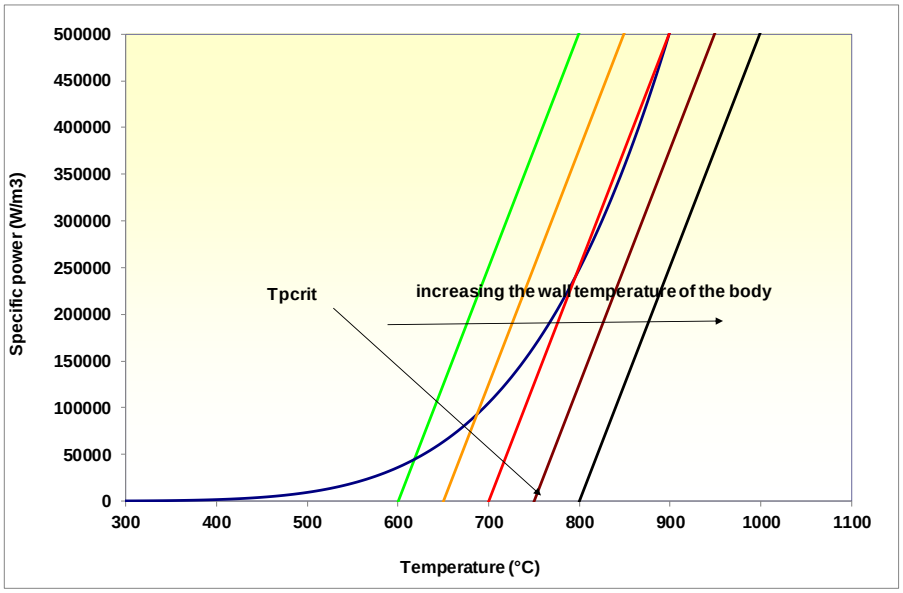

Figure 16 – Hot surface ignition of a stoichiometric hydrogen-air mixture for different sizes of the hot body using self-ignition theory

According to this same model, T_{pcrit} varies significantly with the size of the hot body (Figure 17) dropping to the standard AIT for D = 50 mm (which was expected given that the theory is behind). It compares reasonably with the experimental data.

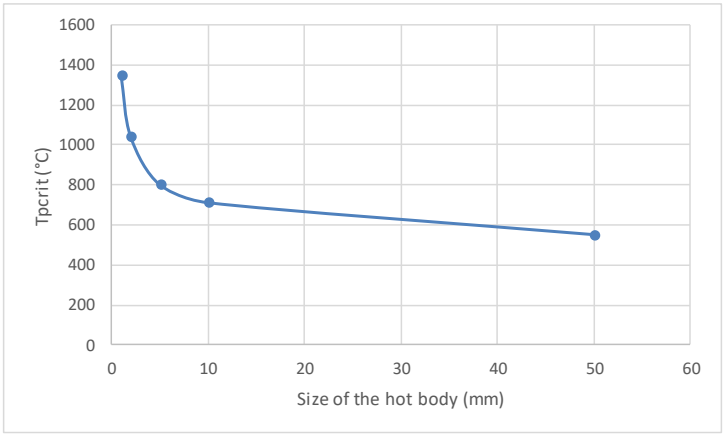

Figure 17 – Evolution of Tpcrit with D for a stoichiometric hydrogen-air mixture

Nevertheless, as pointed out by Laurendeau [56], self-ignition theory is only a necessary condition to observe some burning in contact with the heated surface. It is not "sufficient" to decide whether the flame will be able to propagate away throughout the mixture. This is the object of present research (Proust, 2019) [64] and is discussed further below.

3.3.3 Further theoretical approaches

Physically, the auto-ignition process could be formulated as a thermal explosion phenomenon in a non-adiabatic reacting system. When chemical energy release dominates the competition between chemical reaction heat release and heat losses to the surrounding, ignition takes place. According to Semenov's theory of thermal explosion (Semenoff, 1928) [65] and Frank-Kamenetskii [66] theory about heat conductivity in a system (Frank-Kamenetskii, 1955) [66], the temperature dynamics in a closed non-adiabatic vessel filled with a combustible mixture can be expressed in the form:

$$\rho \cdot c_P \cdot \frac{\partial T}{\partial t} = -\rho \cdot c_P \cdot u \cdot \frac{\partial T}{\partial x} + k \cdot \frac{\partial^2 T}{\partial x^2} + r \cdot Q \qquad \textit{(Eq. 14)}$$

where T is the temperature of the combustible gas mixture, u is a convective velocity, ρ and c_p are the gas density and specific heat capacity, r is the chemical reaction rate, and Q is the energy of combustion. Assuming convective heat transfer with no radiation the balance equation can be written as follows:

$$\rho \cdot c_P \cdot \frac{\partial T}{\partial t} = -\frac{hA}{V}(T - T_\infty) + r \cdot Q =: -q_L + q_R, \qquad \textit{(Eq. 15)}$$

where h is the heat transfer coefficient, A/V is the ratio of area to volume of the system, T_∞ is the ambient temperature. The chemical reaction rate in the simplest way for a one step chemical reaction in Arrhenius form is:

$$r = k_0 [H_2]^a [O_2]^b \exp\left(-\frac{E_a}{RT}\right) \qquad \textit{(Eq. 16)}$$

where E_a is the activation energy, $[H_2]$ and $[O_2]$ are the reacting component concentrations, and k_0 is the pre-exponential factor. The reacting mixture temperature depends on the ratio between the combustion heat release term q_R and the heat loss term q_L. Figure 18 schematically shows the thermal balance diagram of a reacting system close to the auto-ignition point which can be used for analysing the possibility of auto-ignition.

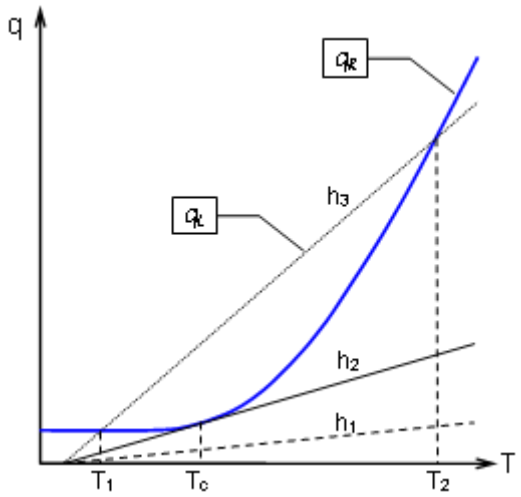

Figure 18 - Thermal balance diagram for a combustible system with different heat losses h_i

Considering a system with constant heat release rate and different heat losses with various heat transfer coefficients h ($h_3 > h_2 > h_1$), the heat loss function q_L depends linearly on temperature. Because the chemical energy release depends exponentially on temperature, q_R will be larger than q_L when temperature is sufficiently high. Beyond this temperature, the temperature will further rapidly increase due to the self-heating process. For a low heat transfer coefficient h_1, the heat generation function q_R is always greater than the heat losses q_L. In this case, auto-ignition always occurs. The critical conditions for heat transfer coefficient h_2 can be found such that $q_R = q_L$ and $dq_R/dT = dq_L/dT$ at a critical temperature T_c. The temperature at this point is called the auto-ignition temperature or minimum temperature at which auto-ignition will occur. This point corresponds to an equilibrium state between heat release and heat losses in a combustible system. A slight increase in temperature will trigger the ignition.

Further decreasing the heat transfer coefficient $h = h_3$ will inhibit the auto-ignition if the mixture temperature is less than the temperature at the onset of self-heating (T_2). At temperature T_1 the system is stable: a slight increase in T will lead to $q_L > q_R$ and the system temperature will return to T_1. Similarly, a slight decrease in T will lead to $q_L < q_R$ and consequently the temperature will increase and return to T_1. The system is unstable at T_2 as a slight perturbation in temperature will shift the temperature away from T_2.

The influence of the gas volume size can also be interpreted using the thermal balance diagram as shown in Figure 18. For a cylindrical surface with a radius R, the temperature evolution will depend on chemical heat release and heat losses in the form:

$$\rho \cdot c_P \cdot \frac{\partial T}{\partial t} = -\frac{h}{R}(T - T_\infty) + r \cdot Q \qquad \textit{(Eq. 17)}$$

where R is the radius of a cylinder surface. The chemical reaction rate remains the same as in Eq. 16.

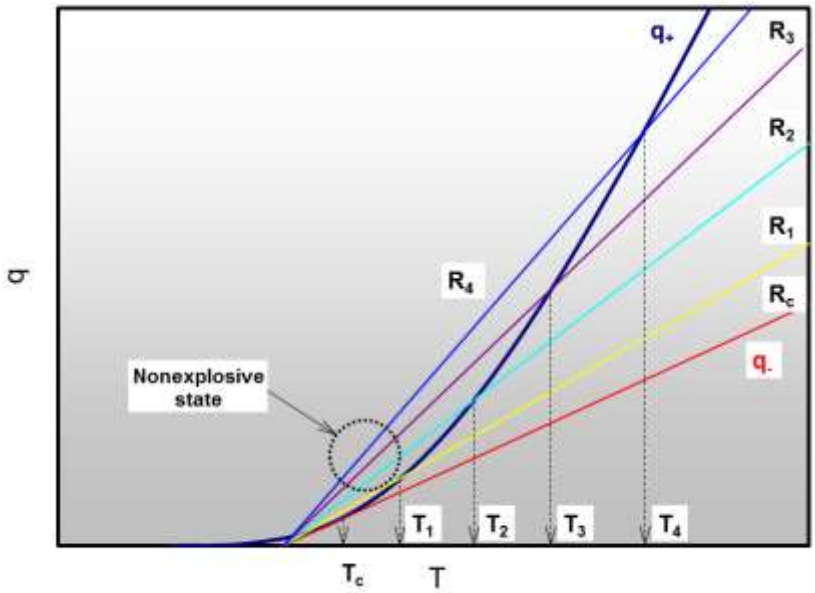

Figure 19 - Thermal balance in a cylindrical pipe with different radii. $R_c > R_1 > R_2 > R_3 > R_4$

As Eq. 17 shows, decreasing the radius of a tube increases the heat loss efficiency. In this case, an increase of the self-ignition temperature can be expected. Figure 19 shows the relative displacement of self-ignition temperature due to decreasing pipe radius:

$R_c > R_1 > R_2 > R_3 > R_4 \leftrightarrow T_c < T_1 < T_2 < T_3 < T_4$

The pipe radius R_c corresponds to the critical (minimum) self-ignition temperature T_c for a larger tube radius at the point of tangential line of heat losses to the heat release line.

Figure 20 shows quantitatively the dependence of self-ignition temperature T_c versus cylindrical pipe radius as calculated for a typical activation energy E_a/R = 4000 K for hydrogen-air mixtures. With a radius changing from 10 to 25 mm the self-ignition temperature decreases from 1550 K to 735 K. Hence, in the planned experiments a reduction of the self-ignition temperature can be expected for a large scale cylinder surface.

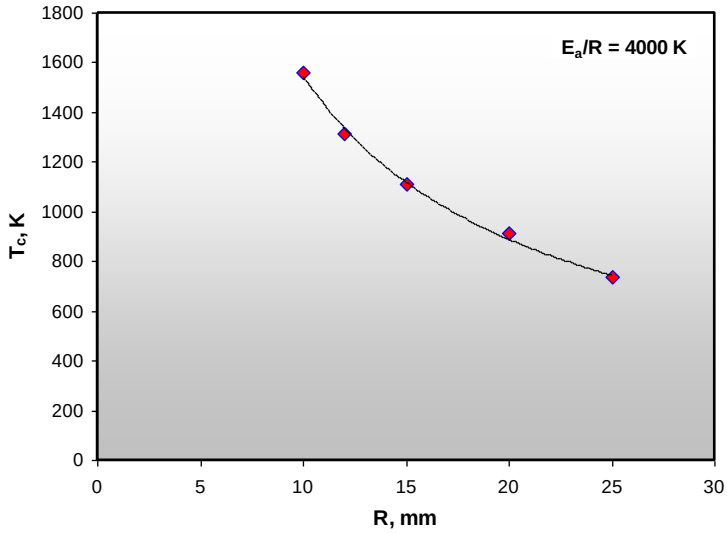

Figure 20 - Calculated self-ignition temperature in a cylindrical vessel of different radius R

Ignition in a hydrogen-oxygen system is a well-known process since the detailed reaction mechanism for hydrogen-oxygen mixtures is relatively well understood. There are many experiments and calculations on ignition in this system at different initial pressures and temperatures. Experimental data are mainly known for pure hydrogen-oxygen mixtures at pressures lower than 1 bar and at elevated temperatures (Lewis, von Elbe, 1987) [67]. Figure 21 shows the so called "three explosion limits diagram" for a stoichiometric hydrogen-oxygen mixture as function of initial pressure and temperature. The first explosion limit at very low pressures below 0.3 bar depends on the size of the vessel and is sensitive to quality of the wall. At such low pressures, the probability of radical-to-wall collision is much higher than radical-to-radical or radical-to-molecule collision. Thus, at very low pressures, below the first explosion limit, no explosion occurs because radical termination at the wall. Reactions:

H` → wall	termination
O`` → wall	termination
OH` → wall	termination

dominate radical generation supporting the chain reactions. At higher pressure, between the first and the second explosion limits, a branching of chain reactions dominates and the mixture starts to explode at proper temperature (above 400 °C):

H` + $O_2$ → OH` + O``	branching
OH` + $H_2$ → H` + H_2O	propagation
O`` + H_2 → OH` + H`	branching
OH` + $H_2$ → H` + H_2O	propagation
H` + O2 + 3 $H_2$ → 3 H` + 2 H_2O	total

Thus, due to the chain branching one hydrogen radical produces three radicals which lead to explosion after several steps of branching.

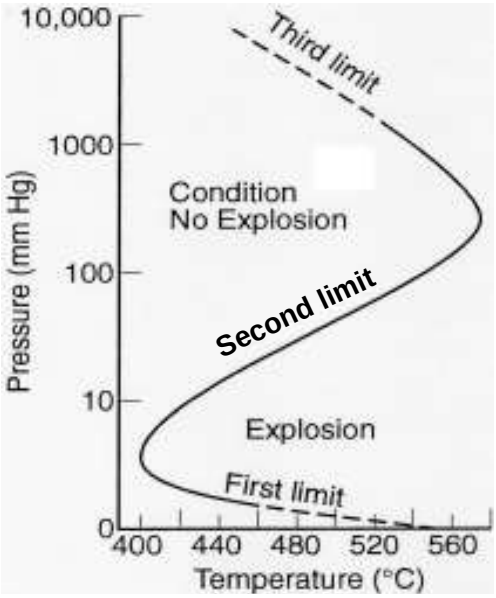

Figure 21 - Three explosion limits diagram for stoichiometric hydrogen-oxygen mixtures [Lewis, von Elbe, 1987]

Further pressure increase, between the second and the third explosion limits, again terminates the chain reactions but now due to three body molecular reactions:

$H` + O_2 + M \rightarrow HO_2` + M$ termination

The mixture does not explode in this domain. With further pressure rising above the third explosion limit the chain reactions

$HO_2` + H_2 \rightarrow H` + H_2O_2$ initiation

$2\ HO_2` \rightarrow H_2O_2 + O_2$ termination

$H_2O_2 \rightarrow 2\ OH`$ initiation

become more important. As the pressure increases again, the initial densities of the reactants increase and a lower temperature is necessary for the reactions to become fast enough for explosion. Furthermore, it can be observed that the effect of temperature is much stronger than that of pressure, which is predicted correctly by the consideration of simplified one-step Arrhenius chemistry. The heat release competes with heat losses on walls at high pressure. Thus, the system becomes more sensitive to the size of reaction volume.

The first and second limits correspond to conditions of very low pressures (up to an absolute pressure of about 0.3 bar) and will not be considered here. The self-ignition temperatures at ambient pressures of 1 bar at the position of the so-called “third explosion limit” can now be calculated.

Numerical calculations

To calculate self-ignition temperatures for different hydrogen-air mixtures starting from cryogenic initial temperatures the Cantera (Goodwin, 2009) [68] and INSFLA codes (Maas, 1988) [69] were used. Cantera is an open-source, extensible software suite for CVD process simulations. It has a routine for zero-dimensional calculations of induction time delay or for self-ignition temperature evaluation. The code was created at the University of Heidelberg and Karlsruhe University in order to simulate unsteady 1D laminar reacting flows like laminar flames, ignition processes, counter-flow systems and pipe flows.

INSFLA is able to compute time and space dependent solutions for species concentrations, velocity, pressure, temperature and density provided that correct reaction mechanisms, species data and suitable options are chosen. The available options include calculation of isothermal or adiabatic systems, different geometrical and flow conditions. It is also possible to choose constant or variable pressure conditions. For the present work the option "auto-ignition in closed vessels (cylindrical), including the destruction of radicals at the surface" was used.

Two hydrogen/oxygen/(nitrogen) mechanisms were chosen: (1) the Lutz mechanism (Lutz, 1988) [70], and (2) the Maas-Warnatz mechanism (Maas, Warnatz, 1988) [50]. For each reaction, the reaction rate was given in Arrhenius form:

$$k = A \cdot T^n \cdot \exp\left(-\frac{E_a}{R \cdot T}\right)$$

(Eq. 18)

Both two mechanisms are listed in Appendix A. These mechanisms use the same 9 species (H_2, O_2, N_2, H, O, OH, HO_2, H_2O, H_2O_2) and 20 (Lutz, 1988) [70] or 37 (Maas, Warnatz, 1988) [50] elementary reactions with Arrhenius kinetics. They practically agree in 14 reactions and differ in other reactions. The Arrhenius constants differ for both mechanisms. Third body (wall) reactions are also different for both mechanisms.

Using the Cantera code in a zero-dimensional approach one can see an evident difference between the Lutz (1988) and Maas-Warnatz (1988) mechanisms (Figure 22). First of all, the Lutz mechanism shows almost no influence of mixture reactivity or hydrogen concentration on critical auto-ignition temperature. The only slight difference of about 5 degrees is in vicinity of the LFL. For the Maas-Warnatz mechanism, the auto-ignition temperature changes from 895 K at the LFL to 820 K at the UFL. Selecting the most appropriate mechanism would require comparison with experimental data.

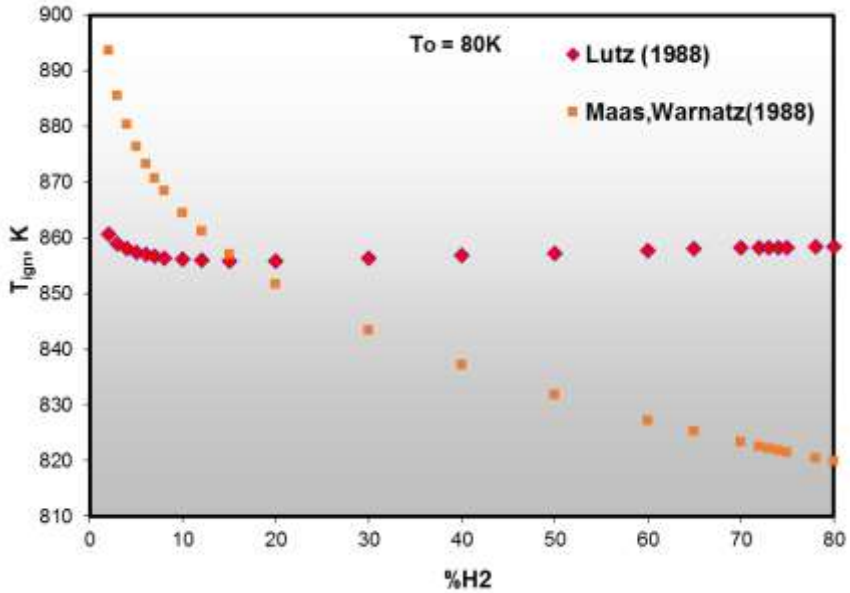

Figure 22 - Calculated auto-ignition temperatures T_i for different hydrogen-air mixtures at cryogenic temperature T_∞ = 80 K and 1 s of ignition time delay (Maas-Warnatz mechanism against Lutz mechanism).

Compared to the zero-dimension Cantera solution, the advantage of INSFLA code is the ability to calculate a chemical reactor state with its dimensions as function of a residence time for a combustible mixture. In reality, it may be that experimental data are in between

the calculations using zero-dimension and 1D models, because the effect of geometry can be overestimated and also characteristic induction time can be too short for the system to react on the effect of heat losses (Vandebroek, 2001) [71]. Figure 23 shows an example of calculated temperature profile in a chemical reactor of 15 mm ID filled with a gas mixture diluted with 40% steam at 70 bar initial pressure and a temperature of 640 K. A significant temperature rise of the mixture in such a reactor indicates the self-ignition process. The temperature of the mixture increases from initial value of 640 K to 3100 K after 36.9 s of residence time. Reducing the initial temperature by only 5 degrees completely alters the reactor behaviour. The mixture temperature does not change within several hours of residence time. This implies that for this mixture at a pressure of 70 bar temperature of 640 K can be taken as the critical self-ignition temperature *T*c.

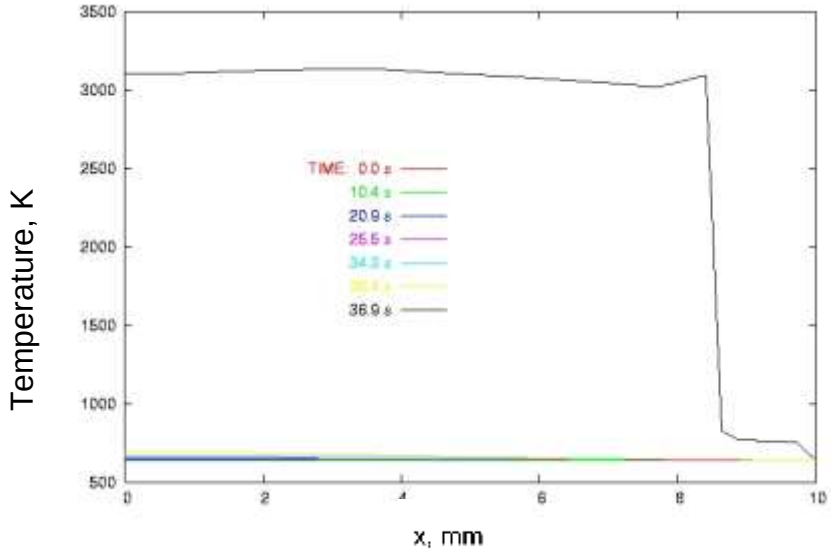

Figure 23 - Calculated temperature distribution in a chemical reactor filled with hydrogen-oxygen mixture (40% H_2O) at 70 bar of initial pressure and 640 K of initial temperature

The same calculations have been performed using INSFLA code with Maas-Warnatz mechanism for hydrogen – oxygen and hydrogen –air mixtures at ambient conditions (P = 1 bar and T = 300 K). Figures 24 and 25 show the calculated self-ignition temperatures for both compositions (points) as function of hydrogen concentration. Blue lines indicate the flammability limits as function of initial temperature. Both pictures show that the self-ignition limits calculated using the Mass-Warnatz mechanism practically do not depend on hydrogen concentration except the points in vicinity of the flammability limits. The calculations fit very well to the experimental data of different researchers. Moreover, similar to the theoretical analysis presented in Figure 20, the highest values of self-ignition temperature (594°C) corresponds to a smaller diameter of cylinder surface (Ziskin, 1942) [72].

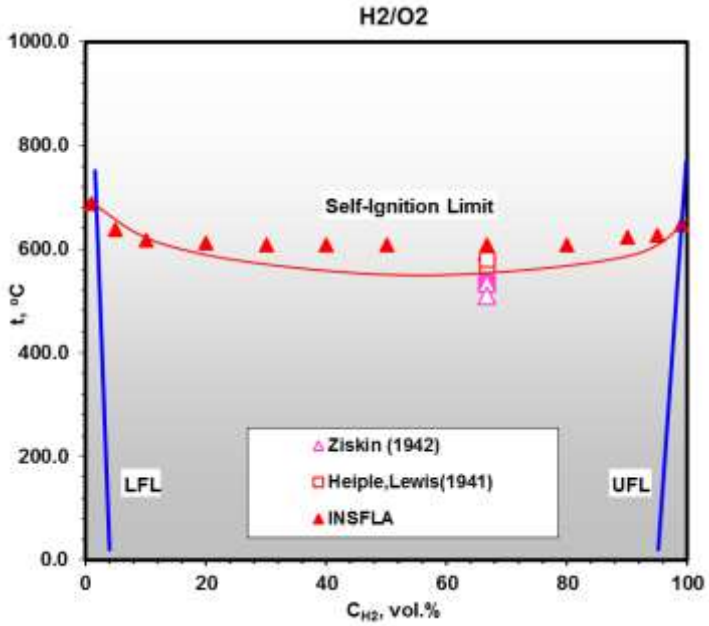

Figure 24- Calculated auto-ignition temperatures T_i for different hydrogen-oxygen mixtures at ambient initial temperature T_∞ = 300 K (Maas-Warnatz mechanism)

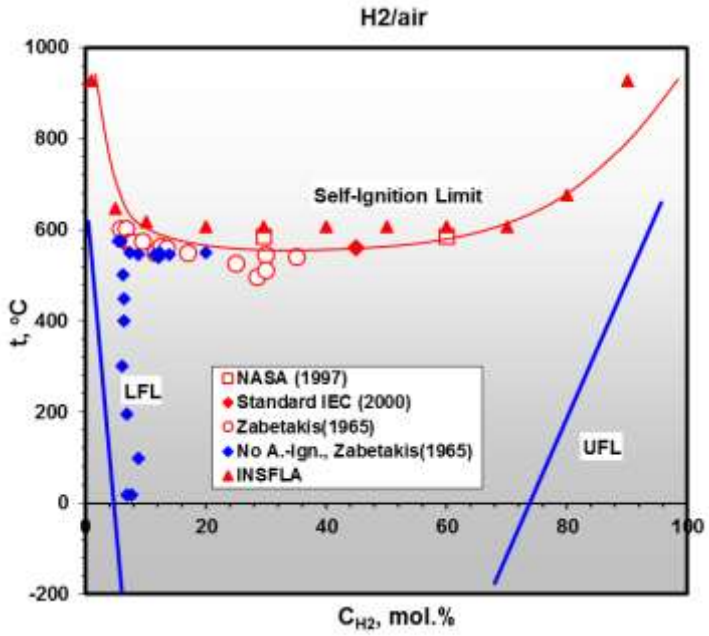

Figure 25 - Calculated auto-ignition temperatures T_i for different hydrogen-air mixtures at ambient initial temperature T_∞ = 300K (Maas-Warnatz mechanism)

The calculations agree very well with experimental measurements on auto-ignition temperature under hot surface ignition of hydrogen – air mixtures performed at INERIS by Proust (2019) [73] (Figure 26). For instance, the calculations with Maas-Warnatz mechanism give an auto-ignition temperature *T*c = 607°C for stoichiometric hydrogen-air mixture. INERIS data give the value *T*c = 630°C. Compared to the calculations, the INERIS measurements show a slightly increasing auto-ignition temperature from 595°C to 645°C with hydrogen concentration increase from 10% to 70% H_2 at ambient initial conditions.

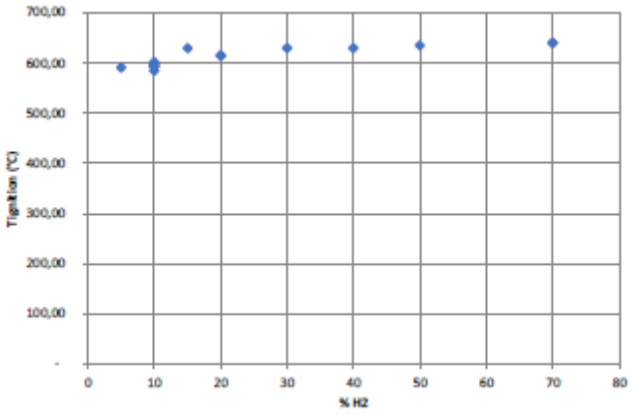

Figure 26 - Influence of the proportion of H_2 in the mixture on the hot surface ignition temperature (ambient conditions at rest)

Both theoretical calculations (Figure 27, right) and INERIS experimental data (Figure 27, left) demonstrate no dependence of auto-ignition temperature versus initial temperature of the gas. The experimental auto-ignition temperature difference less than ±5 degrees was within the accuracy of experiments with initial temperature changing down to -130°C. Calculated auto-ignition temperature difference was almost negligibly small ±0.02 degrees with initial temperature changing from ambient to 80 K. The only difference was between two mechanisms T_{ign} = 591.22°C (Maas-Warnatz) and T_{ign} = 582.90°C (Lutz).

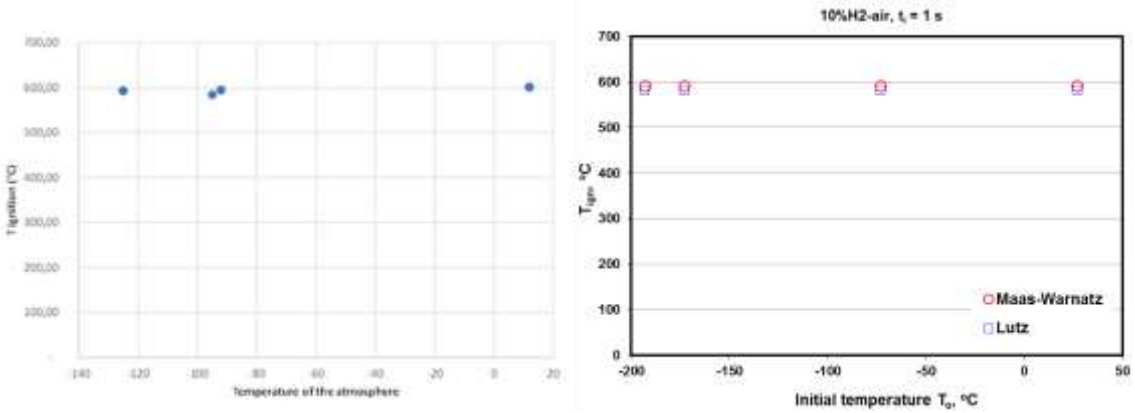

Figure 27 - Influence of the temperature of the H2 – air mixture on the hot surface ignition temperature (10% H2): INERIS experiments (left); calculations for t_i=1s (right)

To conclude, theoretical calculations of auto-ignition temperatures for different hydrogen-air compositions were performed using INSFLA and Cantera codes with two mechanisms (Lutz (1988) and Maas-Warnatz (1988)). It was shown that initial temperature of the gas does not affect the calculated auto-ignition temperature even being reduced to 80 K.

Hydrogen concentration has an insignificant influence on auto-ignition temperature within the flammable domain (10-70% H_2 in air). The only a difference of 200-300 K occurs beyond the flammability limits at 2% H_2 and 90% H_2 in air.

Theoretical calculations fit very well to the experimental measurements performed by INERIS [75] with respect to the effect of hydrogen concentration and cryogenic initial temperature up to 140 K.

3.4. Charge generation and accumulation resulting from LH2 emerging from a leak point, and flowing in pipes

The LH2 may accumulate charge as it flows in pipes, although this would not present an ignition hazard within the pipes or receiving vessels providing that no air or oxygen is present. Externally to pipes and vessels, electrostatic discharges can be avoided by providing earthed, conducting pipework and vessels.

However, charged clouds may form when LH2 emerges from a leak (such as a hole in a pipe), and this may create an ignition hazard as the hydrogen mixes with the air to form a flammable mixture. The charged clouds could potentially consist of liquid hydrogen and liquefied or solidified water vapour (such as ice formed at the leak point subsequently breaking off) or condensed components of the air itself. Charged clouds may result in ignition by a number of mechanisms such as: inducing hazardous potentials on isolated conductors (for example, lumps of ice), promoting corona discharges even from earthed surfaces, or lightning-type discharges if the charged cloud is large enough. Experiments in the framework of the PRESLHY project have shown that cold gas jets generated relatively strong electric fields [74]. This charge is thought to have been generated by the formation and subsequent break-up of solid material around the release orifice. Currently, it is unclear what the composition of the solid material is, and how this relates in practice to the measured charge levels.

Experiments will be carried out to try to measure the charging of LH2 in pipes, and also to understand the formation of charged clouds in the event of a leak.

The following sections describe a number of methods that may be employed to measure these phenomena and the pros and cons are discussed.

Measurement of electric field and charge density in cloud formed from a leak point

It is anticipated that a multi-phase jet of LH_2 / condensed materials will carry some degree of electrostatic charge as indicated in previous studies conducted by Cassutt et al [75] and KIT (Necker 2019) [76], as part of the PRESLHY project. Charging of this multi-phase jet could arise from tribo-charging of the liquid hydrogen within the pipe before release, charge separation occurring at the release nozzle, polarisation and charge separation of droplets during break-up, and tribo-charging of the droplets / particles against each other.

Unfortunately, the results of Cassutt are difficult to interpret for different system geometries as the experimental conditions and measurement methods are not clearly described. However, initial results obtained from KIT (as part of the PRESLHY project) using LH_2 at 110 – 130 K yielded electric field measurements that can be interrogated in order to assist in the design of electric field measurement systems for the larger scale experiments at HSL.

Field measurements in open air

In the KIT Tests, a jet of cold gaseous H_2, released from ca. 9 bar through a 1 mm hole created a field of the order of 100 V/m at a distance, r, of 0.5 m from the axis of the jet (at a range of positions along the jet length). The jet included condensates such as ice, oxygen etc., from the surrounding air. The measured field can be analysed by assuming that the jet acts as a uniformly charged cylinder. Since the field measurement was made outside of the

charged jet then, assuming the length is long compared to the radius, the field is estimated as:

$$E = \frac{\lambda}{2\pi\varepsilon_0\varepsilon_r r} \qquad \textit{(Eq. 19)}$$

Where: E = electric field (V m^{-1})

λ- = charge per unit length (C m^{-1})

ε_0 = permittivity of free space (ca. 8.85 x 10^{-12} F m^{-1})

ε_r = relative permittivity of air

r = distance from axis of cylinder (m)

The value for the relative permittivity of air (and many gases) is very close to 1 at room temperature, due to the low density and hence small effect on the applied field, and is not expected to be larger at lower temperatures (a value of less than 1 is physically impossible). Therefore a value of 1 has been used in these calculations.

Using Equation 19, the KIT results indicate that the charge per length was ca. 10^{-9} C m^{-1}. Assuming a jet radius of ca. 0.5 m gives a charge density of ca. 10^{-9} C m^{-3} of the jet (cloud). The mass flow rate being used in the KIT experiments was of the order of 1 g per second.

The flow rate in the proposed HSL experiment will be several hundred times higher than that in the KIT study, although the larger nozzle sizes may serve to reduce the degree of charging that takes place due to there being a smaller wall area available per unit volume of liquid. It is predicted that a charge per unit length of the jet in the HSL experiments may lie somewhere between those from the KIT tests and several orders of magnitude higher. If the field is measured at 1 m from the axis of the jet then a field of hundreds or thousands of V/m could be expected, i.e. between 10^{-9} and 10^{-6} C per metre.

Experiment 1: Field Meter

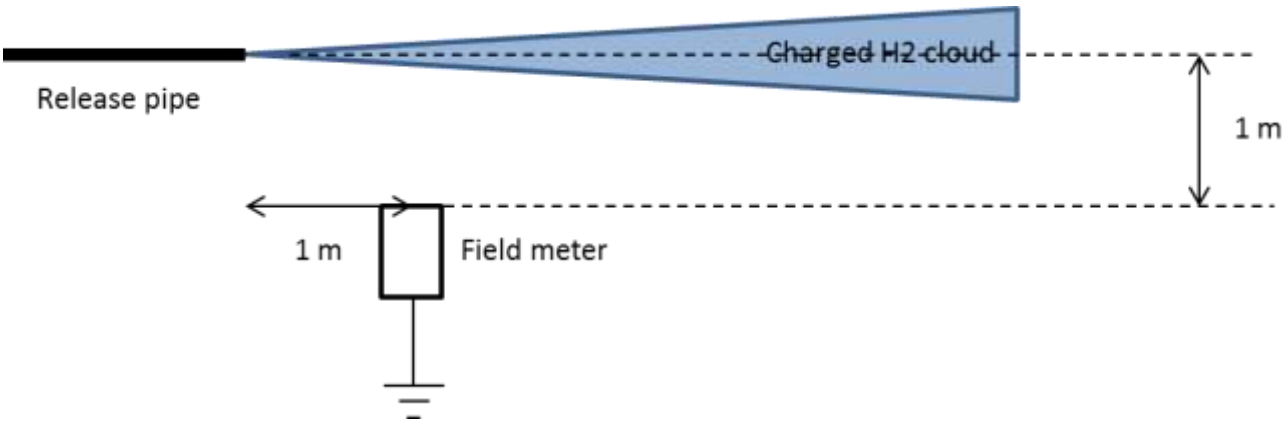

Figure 28 – Diagram of electrostatic measurements of LH2 using a field meter.

Measuring the field in this way would give only a crude assessment of the charge density, due to the influence of other earth planes such as supporting structures, the field mill itself, and the ground. However, it will be easier to implement and should be adopted initially to observe whether electrostatic charge is of a magnitude to give cause for concern.

Experiment 2: Faraday Pail

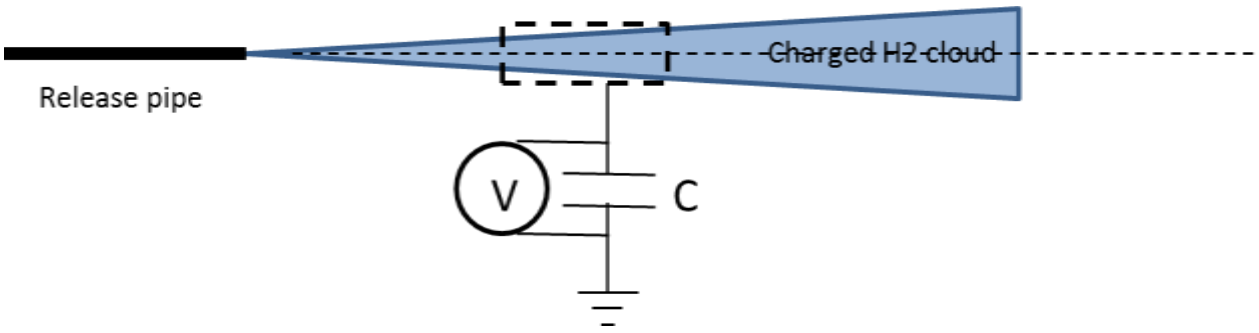

Figure 29 – Diagram of electrostatic measurements of LH_2 using the Faraday pail principle.

A more sophisticated method of determining charge density is to pass the charged cloud through an open- ended cage and measure the voltage induced on the cage. The charge could then be measured directly using an approximation of the Faraday pail principle, i.e. the voltage induced on the cage is proportional to the charge on the material within it, as given by the relationship:

$$V = \frac{Q}{C} \qquad \textit{(Eq. 20)}$$

Where Q = charge on material within the cage (C)

C = capacitance of the cage arrangement (F)

V = voltage induced on cage (V)

Assuming a cage of 1 m length, the charge within it may be 10^{-9} to 10^{-6} C, based on the initial results from KIT, as explained above. An isolated cage on its own would have a low capacitance and may reach a hazardous potential. For example, taking an expected capacitance of no more than 100 pF for an object of that size, then an enclosed charge of 10^{-6} C would induce a voltage of > 10 kV. To achieve a measured voltage of a few volts (the so called "virtual earth" method to avoid ignition potential), it is anticipated that an additional capacitance of between 10^{-9} F (1 nF) and 10^{-6} F (1 µF) in parallel with the cage will be required. The isolated capacitance will need to be of low charge leakage, i.e. high resistance to earth, including the leakage through the electrometer used so as to monitor the voltage. As illustrated in general terms in Figure 30, the charge collected on a capacitor with leakage to earth will be less than a perfectly isolated capacitor. Assuming the residence time of the cloud within the cage to be about 1 second (e.g. passing through 1 m length at 1 m/s), the time constant of the measurement circuit, τ, given by the product of

the capacitance and the resistance to earth will need to be a considerably larger than 1 second in order for the losses to be negligible.

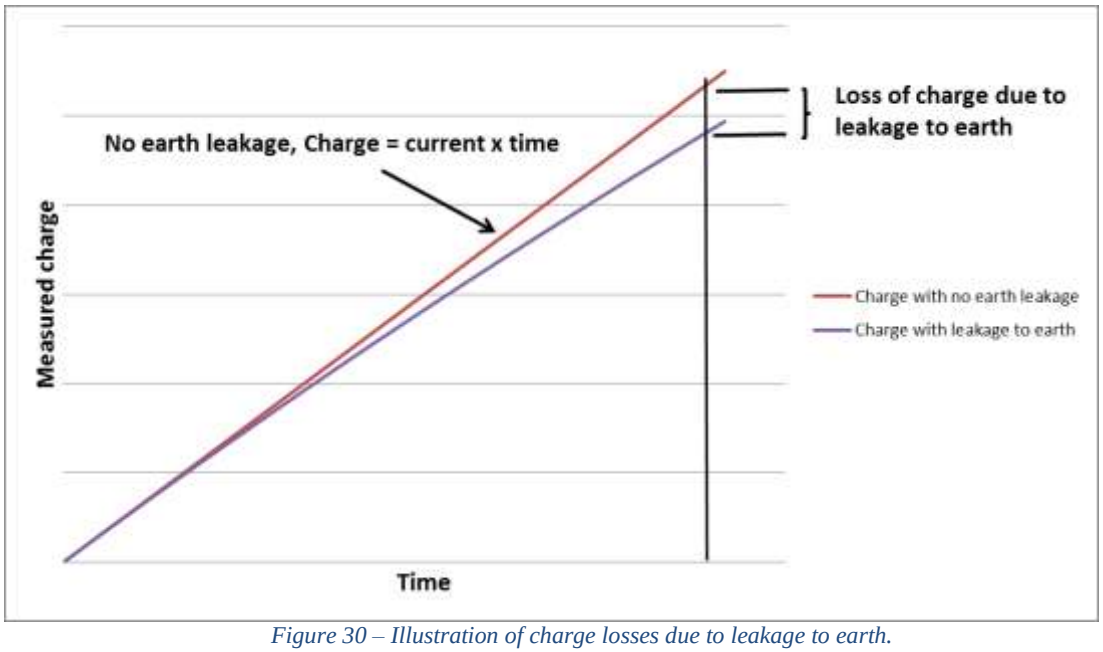

Figure 30 – Illustration of charge losses due to leakage to earth.

$$\tau = RC \qquad \textit{(Eq. 21)}$$

And, re-arranging:

$$R = \frac{\tau}{C} \qquad \textit{(Eq. 22)}$$

For a loss of charge no more than 1%, it can be shown, by comparing charge accumulation in completely isolated cage with that obtained with a leakage path to earth, that a time constant of approximately 60 seconds would be required, i.e. 60 times longer than the 1 residence time.

Assuming a capacitance of 10^{-9} F s minute, the resistance to earth would need to be no more than $60/10^{-9} = 6 \times 10^{10}$ ohms. For a higher capacitance of 10^{-6} F, a lower resistance of 6×10^{7} ohms could be acceptable. However, it may prove difficult to maintain such a high resistance to earth for outdoor conditions where rain and condensation are likely.

Another potential issue with this method is that impingement of the cloud with the cage could cause charge transfer that would cause a voltage on the cage in addition to the voltage induced, though it should be able to distinguish between these the two effects providing the direct charging does not significantly exceed the induced charging. The voltage induced by the charged fuel will be temporary and only present while the charged jet resides within the cage. Any charging caused by direct impingement will cause a permanent voltage to be present. This is shown in Figure 31.

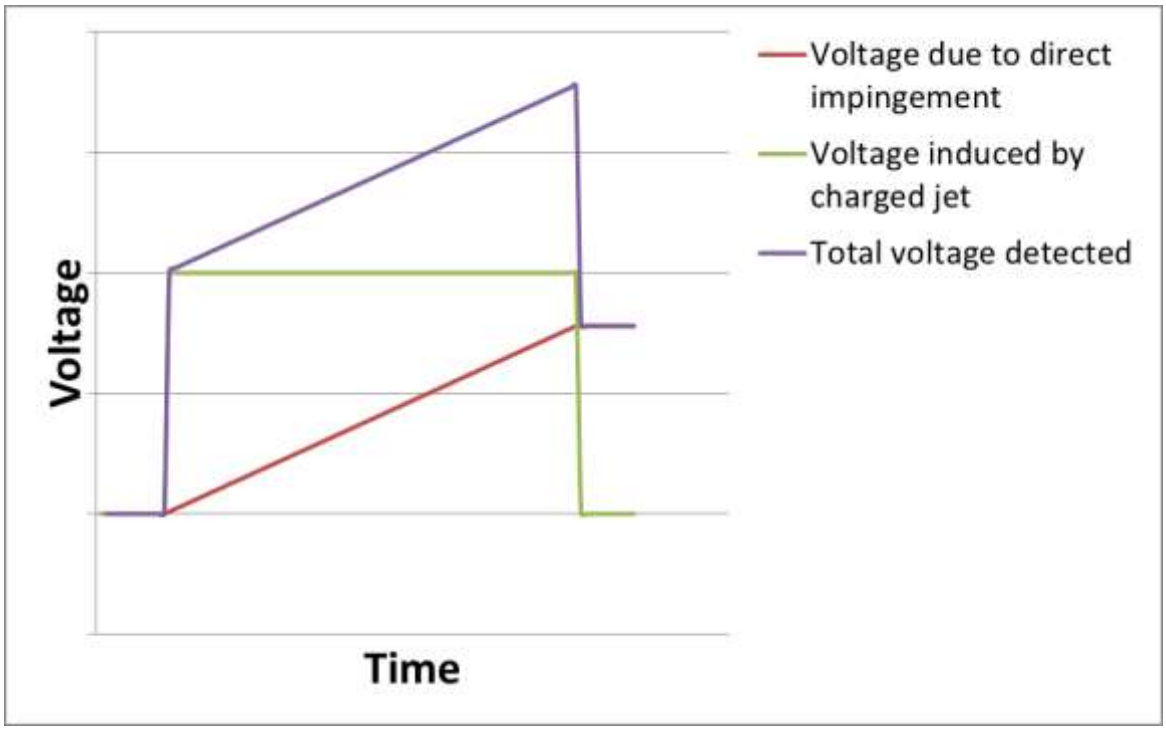

Figure 31 – Illustration of induced voltage, and permanent voltage if jet impinges on cage.

Experiment 3: Field measurements at wall of earthed cage

Another means of employing a cage is to earth it and use a field meter to measure the field caused within the cage by the cloud within it.

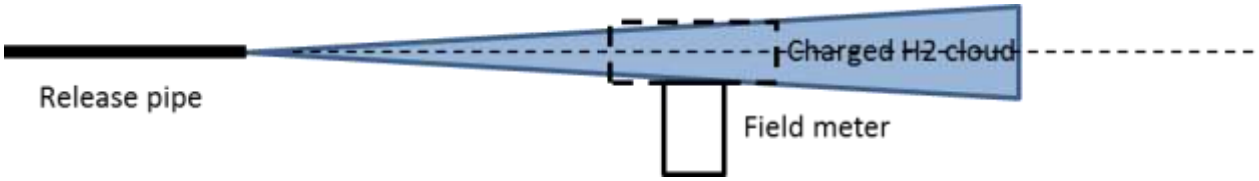

Figure 32 – Diagram of electrostatic measurement of LH_2 using an earthed cage.

Assuming a uniform charge density within a cylindrical cage (a crude approximation) then the field at the cage wall would be given by:

$$E = \frac{\sigma R}{2\varepsilon_0 \varepsilon_r} \qquad \textit{(Eq. 23)}$$

Where σ = charge density (C m^{-3})

R = radius of the cage (m)

ε_0 = permittivity of air (ca. 8.85 x 10^{-12} F m^{-1})

ε_r = relative permittivity of the cloud, which will be approximately = 1

An advantage of this method is that the cage is earthed and therefore, it is not necessary to achieve an onerous level of electrical isolation.

In order to estimate end effects, it will be necessary to calibrate the set up using a conducting rod placed through the axis of the cage and raised to ca. 1 kV. The actual measured field can then be compared with the theoretical field that would occur in an infinitely long cage.

Due to the potential difficulties of maintaining isolation of isolated sections, it is proposed that using an earthed cage and monitoring the field will be the most effective method.

Measurement of current due to flow along pipe

As liquid hydrogen flows through a pipe before release it will become charged due to the interaction with the pipe wall. The liquid will charge as it progresses along the pipe until it reaches a maximum charge density (charge per unit volume). The charge density multiplied by the flow rate of the liquid results in a measurement of current (i.e. charge per second i.e. Amps), known as the streaming current. The degree of charging is dependent upon many variables. However, for insulating liquids, a summary of the work of several researchers (Cross 1987) [77] shows that the maximum streaming current carried by the turbulently flowing liquid would be defined by a function of the form:

$$I_\infty = K d^\alpha v^\beta \qquad \textit{(Eq. 24)}$$

Where I_∞ = streaming current after travelling an infinite distance along the pipe (A)

d = internal pipe diameter (m)

v = velocity of liquid in the pipe (m s^{-1})

α and β are constants approximately equal to 2

K = a constant equal to 4 µA s^2 m^{-4}

This function is known as the Schon equation.

For experiments planned to be undertaken by HSL (detailed below), it is estimated that the velocity of liquid hydrogen in a 1 inch pipe will be between 2 ms^{-1} and 12 ms^{-1}. These would result in maximum streaming currents within the experiments of 0.01 µA and 0.37 µA.

As stated above, the degree of charging (and hence streaming current) increases as the liquid flows along the pipe, as illustrated in Figure 31.

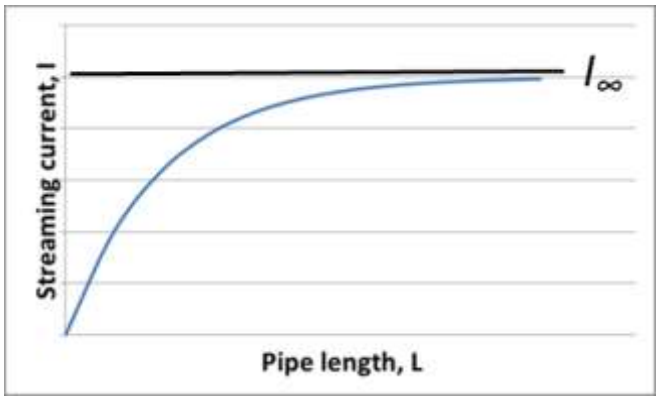

Figure 33 – A graph of current against pipe length.

The streaming current at distance, L, along the pipe can be expressed as a proportion of the maximum streaming current, I_∞, using the relationship:

$$I_L = I_\infty(1 - e^{\left(-\frac{L}{v\tau}\right)}) \qquad \textit{(Eq. 25)}$$

Where: I_L = streaming current after travelling a distance, L, along the pipe (A)

I_∞ = streaming current after travelling an infinite distance along the pipe (A)

v = velocity of liquid in the pipe (m s^{-1})

L = distance along the pipe (m)

τ = relaxation time of the liquid (s), defined by equation 26.

$$\tau = \varepsilon_0 \varepsilon_r \rho \qquad \textit{(Eq. 26)}$$

Where: τ = relaxation time of the liquid (s)

ε_0 = permittivity of air (ca. 8.85 x 10^{-12} F m^{-1})

ε_r = relative permittivity of the liquid

ρ = resistivity of the liquid (Ω m)

The relative permittivity of liquid hydrogen has been reported as 1.23 (Wolfke, 1926) [78] and resistivity reported as no less than 10^{15} Ω m (Cassutt, 1962) [75]. From equations 20 and 21, this gives a charge relaxation time for liquid hydrogen of at least 1090 seconds [*4].

Equation 20 can be re-arranged to calculate the length of pipe corresponding to a chosen fraction of the maximum current, i.e. I_L / I_∞:

$$L = -v\tau \; ln(1 - \frac{I_L}{I_\infty}) \qquad \textit{(Eq. 27)}$$

[*4] Note that insulating liquids, when highly charged, can exhibit a shorter relaxation time than calculated using this method, due to a phenomenon referred to as hyperbolic relaxation.

Substituting the value of 1090 s for τ, and using a velocity of 2 - 12 ms^{-1}, results in a length of many thousands of metres to achieve half of the maximum streaming current. For the proposed length of pipe in the experimental system (including the vacuum insulated hose) of ca. 35 m, the streaming current will peak at only tens of pA. In practice, this will be difficult to measure, especially in an open environment where stray currents due to impact charging from airborne dust etc. may be of a similar order of magnitude. Due to this anticipated lack of accuracy in measuring the current generated within the pipe, experiments will not be carried out to investigate different lengths of pipe; it is anticipated that the differences observed would be so small as to be imperceptible or scientifically undefendable. An attempt could be made to determine either the streaming current by observing the voltage acquired by an isolated section of pipe, calculating the charge on the liquid within, and relating the two using the relationship given in equation 10 (having measured the capacitance of the pipe section as it is mounted within the experimental arrangement). However, due to the difficulties anticipated in achieving and maintaining a suitable level of electrical isolation for the section of pipe, this methods has not been adopted (see the above section on the charged plume for further discussion of the difficulties).

As an alternative method of investigation, an attempt could be made to determine the wall current. The wall current is a measure of the rate of charge transfer to the pipe from the liquid during transit through it. While this does not give a measure of the streaming current, and would be expected to be even smaller in magnitude that the streaming current, it does give an indication of how much charge transfer is taking place within the isolated pipe section. Wall current can be simply measured by measuring directly the current to earth from an isolated section of pipe. Using an electrometer with a very low input impedance to measure the current imposes a far lower burden on the degree of isolation required. The acceptability of the measurement method can be checked by "injecting" a known current from a calibrated source onto the isolated section of pipe. If the measured current matches the injected current then the amount of current leaking to earth via other paths is acceptable.

It is concluded that the best experimental option is to isolate a section of pipe and connect this directly to a low input impedance electrometer and measure the wall current.

Implications for ignition

Once data has been obtained for the degree of charging for releases at cryogenic temperatures, there remains a need to quantify this effect and to relate the charge level to the occurrence of an actual ignition event, i.e. the potential for incendive discharges.

4. Conclusions

In order to facilitate the use of liquid hydrogen (LH_2) outside of typical industrial applications, for example as a fuel for road vehicles, the understanding of certain high risk scenarios needs development. The PRESLHY project aims to address the most relevant and poorly understood phenomena.

The state of the art report (2018) [1] compiled as part of this project identified a number of ignition phenomena relevant to LH_2 release scenarios. Based on that review, three knowledge gaps were identified: the influence of low temperature on the flammability limits of hydrogen gas; minimum ignition energy and ignition energies of cryogenic H_2/air mixtures; and electrostatic charging and ignition of multiphase jets.

The aim of this report has been to review these knowledge gaps and to further develop theoretical approaches to the analysis of ignition of low temperature mixtures. A brief review of LH_2 release scenarios has been undertaken to inform examination of the relevant theoretical aspects of ignition. Analytical and numerical methods have been developed for the prediction of both minimum ignition energy and hot surface ignition as electrical sparks and hot surfaces are fundamental to many practical ignition scenarios. A number of basic approaches for calculating electrostatic charging in flowing LH_2 have also been presented. The theoretical work identified areas for which there remains a lack of detailed experimental data.

There has been a two-way interaction with the PRESLHY experimental programme, in that the theoretical aspects have supported the design of experiments and the experimental programme has helped to address theoretical knowledge gaps.

One such knowledge gap is how minimum ignition energy and hot surface ignition vary with the initial mixture temperature. The behaviour of liquid pools or solid formations that develop during LH_2 releases is also a topic deserving of further study, including ignitions parameters and the interaction between the substances and liquid water.

While a reasonable estimate of charge build-up in flowing liquids and gas streams can be made, there are two main aspects that merit further investigation. That is that at cryogenic temperatures, the process of solid formation and break up of material may introduce an additional charging mechanism. It also remains uncertain how the generation of a charge in a flowing stream can be related to the occurrence of an ignition event.

The PRESLHY experimental programme has therefore been designed to provide information on these phenomena. Numerical and analytical studies will happen in parallel with the experimental series and both will combine to result in contributions to international standards.

5. References

[1]Jallais, S., Bernard, L., Venetsanos, A., Lisseman, R., Hooker, P., Kuznetsov, M., Jordan, T. and Cirrone, D. (2018) State of the art analysis, Pre-normative REsearch for Safe use of Liquid HYdrogen (PRESLHY)
[2]Hooker, P., Willoughby, D.B. and Royle, M. (2011) Experimental releases of liquid hydrogen, 4th Int. Conf. on Hydrogen Safety, San Francisco, CA, USA, paper 160
[3]Venetsanos A.G. (2019) D3.1 Theory and Analysis of Cryogenic Hydrogen Release and Dispersion, Pre-normative REsearch for Safe use of Liquid HYdrogen (PRESLHY)
[4]Giannissi, S.G., Venetsanos, A.G. (2017) Study of key parameters in modeling liquid hydrogen release and dispersion in open environment, International Journal of Hydrogen Energy, vol. 43, pp. 455-467.
[5]Perry, R.H., Green, D.W. (1999) Perry's chemical engineers' handbook. pp. 2582.
[6]Jin, T., Liu, Y., Wei, J., Wu, M., Lei, G., Chen , H., Lan, Y. (2017) Modelling and analysis of the flammable vapor cloud formed by liquid hydrogen spills, International Journal of Hydrogen Energy, vol. 42, pp. 26762-26770.
[7]Veser, A., Kuznetsov, M., Fast, G., Friedrich, A., Kotchourko, N., Stren, G., Schwall, M., Breitung, W. (2011) The structure and flame propagation regimes in turbulent hydrogen jets. International Journal of Hydrogen Energy, vol. 36, pp. 2351-2359.
[8]Schefer, R.W., Evans, G.H., Zhang, J., Ruggles, A.J., Greif, R. (2010) Ignitability limits for combustion of unintended hydrogen releases: Experimental and theoretical results, International Journal of Hydrogen Energy, vol. 36, pp. 2426-2435.
[9]Zabetakis, M.G. and Burgess, D.S. (1961) Research on the hazards associated with the production and handling of liquid hydrogen. US Department of the Interior, Bureau of Mines.
[10]Witcofski, R.D., Chirivella, J.E. (1984) Experimental and analytical analyses of the mechanisms governing the dispersion of flammable clouds formed by liquid-hydrogen spills, International Journal of Hydrogen Energy Vol. 9: 425
[11]Statharas, J.C., Venetsanos, A.G., Bartzis, J.G., Würtz, J., Schmidtchen, U. (2000) Analysis of data from spilling experiments performed with liquid hydrogen, Journal of Hazardous Materials Vol. 77(1-3): Pages 57-75
[12]Wierzba, I., Harris, K., Karim, G. A. (1992) Effect of low temperature on the rich flammability limits in air of hydrogen and some fuel mixtures containing hydrogen, International Journal of Hydrogen Energy, vol. 17 (2), pp. 149-152.
[13]Zabetakis, M. G. (1965) Flammability characteristics of combustible gases and vapours, Bulletin 627, U.S. Bureau of Mines.
[14]Karim G. A., Wierzba, I., Boon, S. (1984) The lean flammability limits in air of methane, hydrogen and carbon monoxide at low temperatures, Cryogenics: 24, pp. 305-308.
[15]Liaw, H.J., Chen, K.Y. (2016) A model for predicting temperature effect on flammability limits, Fuel, Volume 178, Pages 179-187
[16]Verfondern, K., and Dienhart, B., (1996) Experimental and theoretical investigation of liquid hydrogen pool spreading and vaporization, International Journal of Hydrogen Energy, vol. 22, pp. 649-660.
[17]Royle, M. and Willoughby, D. (2014) Releases of unignited liquid hydrogen, HSE Research Report RR986.
[18]Astbury, G.R., Hawksworth, S.J. (2007) Spontaneous ignition of hydrogen leaks: A review of postulated mechanisms, International Journal of Hydrogen Energy, Vol. 32, pp. 2178–2185.
[19]Proust, C. (2019) Fire and explosion safety in hydrogen containing processes: state of the art and outstanding questions, ISFEH09 symposium, Saint Petersburg, Russia.
[20]Lewis, B., Von Elbe, G. (1987) Combustion, flames and explosions of gases: 3rd edition, Academic Press, London, ISBN 0-12-446751-2.
[21]Carleton, F.B., Weinberg, F.J. (1994) Correlating minimum ignition criteria, Proc. R. Soc. Lond. A, 447, 513-520.
[22]Wolanski, P., Wojcicki, S. (1973) Investigation into the mechanisms of the diffusion ignition of a combustible gas flowing into an oxidizing atmosphere, Proc. Combust. Inst., 14, 1217-1223.
[23]Adler, J., Carleton, F.B., Weinberg, F.J. (1993) Ignition of flammable atmospheres by radiation heated fibrous agglomerates, Proc. R. Soc. Lond. A, 440, 1993, 443-460.
[24]Proust, C., Hawksworth, S., Rogers, R., Beyer, M., Lakic, D., Raveau, D., Hervé, P., Pina, V., Petitfrère, C., Lefebvre, X. (2007) Development of a method for predicting the ignition of

explosive atmospheres by mechanical friction and impacts (MECHEX), J. Loss Prev. Process Industries, 20 349-365.
[25] Simon L. H., Fedtke, T., Wilkens, V., Beyer, M. (2013) Incendivity of Ultrasound Applied in Explosive Atmospheres, proceedings 24th ICDERS, Taipei, Taiwan.
[26] Duan, Q., Xiao, H., Gao, W., Wang, Q., Shen, X., Jiang, L., Sun, J.(2015) An experimental study on shock waves and spontaneous ignition produced by pressurized hydrogen release through a tube into atmosphere, Int. J. Hydrogen Energy, 40, 8281-8289.
[27] Kumamoto, A., Iseki, H., Ono, R., Oda, T. (2011) Measurement of minimum ignition energy in hydrogen-oxygen-nitrogen premixed gas by spark discharge, Journal of Physics: Conference Series, 301.
[28] Weinrotter, M., Kopecek, H., Wintner, E., Lackner, M., Winter, F. (2005), Application of laser ignition to hydrogen–air mixtures at high pressures, International Journal of Hydrogen Energy 30(3):319-326
[29] Pratt, T. H. (2000) Electrostatic ignitions of fires and explosions, Center for Chemical Process Safety of the American Institute of Chemical Engineer: 3 Park Avenue, New York, NY 10016-599.
[30] Lewis, B., and von Elbe, G. (1951) Combustion, Flames and Explosions of Gases, First Edition, Academic Press.
[31] Lewis, B., and von Elbe, G. (1961) Combustion, Flames and Explosions of Gases, Second Edition, Academic Press.
[32] Calcote, H.R., Gregory, Jr. C.A., Barnett, C.M., Gilmer, R.B. (1952) Spark ignition. Effect of molecular structure, Ind. Eng. Chem. 44, 2656.
[33] Eckhoff, R. (2002) Minimum ignition energy (MIE) — a basic ignition sensitivity parameter in design of intrinsically safe electrical apparatus for explosive dust clouds, J. of Loss Prev. in the Process Industries, 15, 305-310
[34] Eckhoff, R.K., Ngo, M., Olsen, W. (2010) On the minimum ignition energy (MIE) for propane/air, Journal of Hazardous Materials 175 (2010) 293–29
[35] Kuctha 1986
[36] Ono, R., Nifuku, M., Fujiwara, S., Horiguchi, S., Oda, T. (2007) Minimum ignition energy of hydrogen–air mixture: Effects of humidity and spark duration, Journal of Electrostatics, Volume 65, Issue 2, pp. 87-93.
[37] ISO (2004), Basic considerations for the safety of hydrogen systems, ISO/TR 15916:2004
[38] Glasmann, I. (1977) Combustion, Academic Press, London
[39] Williams, F.A. (1985) Combustion theory: 2nd edition , Benjamin/Cummings publishing company Inc., Amsterdam, ISBN 0-8053-9801-5
[40] Hattwig, M., Steen, H., (2004) Handbook of Explosion Prevention and Protection, Wiley-VCH Verlag GmbH & Co. KGaA, ISBN 9783527307180.
[41] Carleton, F. B., Weinberg F. B. (1994), Correlating minimum ignition criteria, Proceedings of the Royal Society of London. Series A, Volume 447Issue 1931
[42] Coffee, T.P., Kotlar A.J., Miller, M.S. (1983) The Overall Reaction Concept in Premixed, Laminar, Steady-State Flames. I. Stoichiometries, Comb. and Flame, 54, 155-169.
[43] Kuchta, J. M. (1985) Investigation of Fire and Explosion Accidents in the Chemical, Mining, and Fuel-Related Industries A Manual, U.S. Bureau of Mines Bulletin 680.
[44] Kondo, S., Takahashi, A., Tokuhashi, K. (2003) Calculation of minimum ignition energy of premixed gases, Journal of Hazardous Materials, pp. 11-23.
[45] Cantera (2019) Open-source suite of tools for problems involving chemical kinetics, thermodynamics, and transport processes, available at: www.cantera.org
[46] Lamoureux., N., Djebaili-Chaumeix, N., Paillard, C.E. (2002) Laminar flame velocity determination for H2-air-stream mixtures using the spherical bomb method, J. Phys. IV France, 12, pp. 445-458
[47] Kim, H.J., Hong, S.W., Kim, H.D., Yang, S.Y., Chung, S.H. (2001) Quenching Distance Measurement for the Control of Hydrogen Explosion, Proceedings of the 18th International Colloquium on the Dynamics of Explosions and Reactive Systems, Seattle, Washington.
[48] Konnov, A.A. (2008) Remaining uncertainties in the kinetic mechanism of hydrogen combustion, Comb. And Flame, vol.152, pp. 507-528
[49] Brokaw, R.M., Gerstein, M. (1957) Correlations of burning velocity, quenching distances, and minimum ignition energies for hydrocarbon-oxygen-nitrogen systems, Symposium (International) on Combustion, Volume 6, 66-74.

[50]Mass, Ü., Warnatz, J. (1988) Ignition processes in hydrogen oxygen mixtures, Comb. And Flame, vol. 74, pp.53-69.
[51]Bane, S. (2010) Spark ignition: experimental and numerical investigation with application to aviation safety, Dissertation (Ph.D.), California Institute of Technology. http://resolver.caltech.edu/Caltech, THESIS:05272010-173243262
[52]Han, J., Yamashita, H., Hayashi, N. (2011) Numerical study on the spark ignition characteristics of hydrogen–air mixture using detailed chemical kinetics, International Journal of Hydrogen Energy, Volume 36, Issue 15, Pages 9286-9297
[53]Terao, K. (2007) Irreversible Phenomena: Ignitions, combustion and detonation waves, Springer Berlin Heidelberg New York.
[54]Science Direct (2019), Black body radiation, available at: https://www.sciencedirect.com/topics/chemistry/blackbody-radiation [last access: 31.05.2019]
[55]Silver, R.S. (1937) The ignition of gaseous mixtures by hot particles, Phil. Mag. S.7, 23.
[56]Laurendeau, N. (1982) Thermal ignition of methane-air mixtures by hot surfaces: a critical examination, Comb. and Flame, 46, 26-49.
[57]Powell, F. (1969) Ignition of gases and vapors, Industrial and Engineering Chemistry, 61, 29-37.
[58]Kumar, R.K. (1995) Ignitability of Hydrogen/Oxygen/Diluent Mixtures in the Presence of Hot Surfaces, Nuclear Safety, 36, 69-93.
[59]Beyer, M., Markus, D. (2012) Ignition of explosive atmospheres by small hot particles: Comparison of experiments and simulations, Science and Technology of Energetic Materials, 73, 1-7.
[60]Roth, D., Harber, T., Bockhorn, H., Proceedings of the Combustion Institute 36 (2017), 1475-1484
[61]Buckel, J.W, Chandra, S. (1996) Hot wire ignition of hydrogen-oxygen mixtures, Int. J. Hydrogen Energy, 21, 39-44.
[62]Mével, R., Melguizo-Gavilanes, J., Boeck, L.R., Shepherd, J.E. (2019) Experimental and numerical study of the ignition of hydrogen-air mixtures by a localized stationary hot surface, Int. J. of Heat and Fluid Flow, 73, 154-169
[63]Carleton, F., Bothe, H., Proust, C., Hawksworth, S. (2000) Prenormative Research on the use of Optics in Potentially Explosive Atmospheres, Final report U.E contract SMT4-CT96/2104
[64]Proust, C. (2019) Hot surface ignition in flowing streams of hydrogen air mixtures, oral presentation, ICHS, Adelaide, Australia, Sept.
[65]Semenoff, N. (1928) Zur Theorie des Verbrennungsprozesses, Zeitschrift für Physik, 48 571-582
[66]Frank-Kamenetskii, D. (1955) Diffusion and Heat Exchange in Chemical Kinetics. Princeton University Press, NJ.
[67]Lewis, B. and Von Elbe, G. (1987) Combustion, Flames, and Explosions of Gases, Third Edition, Academic Press, Orlando, FL
[68]Goodwin, D. (2009) Cantera: An object-oriented software toolkit for chemical kinetics, thermodynamics, and transport processes, Caltech, Pasadena, [Online]. http://code.google.com/p/cantera
[69]Maas, U. (1988) Mathematical modelling of transient combustion processes using detail reaction mechanisms, PhD thesis, Universität Heidelberg.
[70]Lutz, A.E. (1988) A Numerical Study of Thermal Ignition, Sandia Report SAND88-8228.
[71]Vandebroek, L., Winter, H., Berghmans, J. (2001) Numerical Study of the Auto-ignition Process in Gas Mixtures using Chemical Kinetics. Proceedings of the Safety net Seminar "Combustion Modelling".
[72]Ziskin, M.S. (1942) Zur Zündgrenze dem Knallgas unter atmosphärische Druck, DAN USSR, 34(2): 279
[73]Proust, C. (2019) Summary of experiment series E4.1 results (Ignition parameters), INERIS, an intermediate PRESLHY report,
[74]Friedrich, A., Veser, A., Jordan, T. (2019) Summary of experiment series E3.1 (Discharge) results – part A high pressure. Pre-normative REsearch for Safe use of Liquid Hydrogen (PRESLHY)
[75]Cassutt L., Biron D., Vonnegut B. (1962) Electrostatic Hazards Associated with the Transfer and Storage of Liquid Hydrogen. In: Timmerhaus K.D. (eds) Advances in Cryogenic Engineering. Advances in Cryogenic Engineering, vol 7. Springer, Boston, MA
[76]Personal communication from G. Necker, 28/02/19.
[77]Cross, J.A., Hilger, A. (1987) Electrostatics – Principles, problems and applications, ISBN 0-85274-589-3, Bristol.

[78] Wolfke, M. et al. (1924) On the dielectric constants of liquid and solid hydrogen, Communication No. 171c from the Physical Laboratory at Leiden, (Communicated at the meeting of September 27, 1924)

6. Appendix A

1. Lutz mechanism [Lutz, 1988]:

```
! This is the mechanism from A.E. Lutz, "A Numerical Study of Thermal
Ignition", Sandia Report SAND88-8228 (1988). It is identical to the
mechanism in Lutz, Kee, Miller, Dwyer, and Oppenheim, 22nd Symp. Intl.
Combust. p. 1683.
ELEMENTS
H   O   N
END

SPECIES
H H2 O O2 OH H2O HO2 H2O2 N2

END

REACTIONS                        A          n    Ea,JOULES/MOLE  REFERENCE
H2+O2=2OH                      1.70E+13  0.0    47780.0       ! 135 JAM-BOW
OH+H2=H2O+H                    1.17E+09  1.300   3626.0       ! 136 D-L$W
O+OH=O2+H                      4.00E+14 -0.500      0.0       ! 137 JAM 1986
O+H2=OH+H                      5.06E+04  2.670   6290.0       ! 138 KLEMM,ET
AL 1986
H+O2+M=HO2+M                   3.61E17  -0.72       0.0       ! 139
  H2O/18.6/ H2/2.86/ N2/1.26/
OH+HO2=H2O+O2                  7.5E+12   0.0        0.0       ! 140
H+HO2=OH+OH                    1.4E+14   0.0     1073.0       ! 141
O+HO2=O2+OH                    1.4E+13   0.0     1073.0       ! 142
2OH=O+H2O                      6.00E+08  1.3        0.0       ! 143 COHEN-
WEST.
H+H+M=H2+M                     1.00E+18 -1.0        0.0       ! 144 - orig.
absent
H+H+H2=H2+H2                   9.20E+16 -0.6        0.0       ! 145 JAM-BOW
H+H+H2O=H2+H2O                 6.00E+19 -1.250      0.0       ! 146 JAM-BOW
H+OH+M=H2O+M                   1.60E+22 -2.0        0.0       ! 147 D-L
   H2O/5/
H+O+M=OH+M                     6.20E+16 -0.6        0.0       ! 148 D-L
   H2O/5/
O+O+M=O2+M                     1.89E+13  0.0    -1788.0       ! 149 NBS
H+HO2=H2+O2                    1.25E+13  0.0        0.0       ! 150
HO2+HO2=H2O2+O2                2.00E+12  0.0        0.0       ! 151
H2O2+M=OH+OH+M                 1.3E+17   0.0    45500.0       ! 152
H2O2+H=HO2+H2                  1.6E+12   0.0     3800.0       ! 153
H2O2+OH=H2O+HO2                1.0E+13   0.0     1800.0       ! 154
END
```

2. Maas-Warnatz mechanism [Maas, Warnatz, 1988]:

```
! This is the hydrogen oxidation mechanism from U. Maas & J. Warnatz,
"Ignition Processes in Hydrogen-Oxygen Mixtures", Comb. & Flame, vol.
74, pp. 53-69, 1988.
MECHANISM H2/O2/N2, P = 0.03 TO 50  BAR, HIGH TEMP.REACTIONS
ELEMENTS
H O N END
SPECIES
H2 H O2 O OH HO2 H2O2 H2O N2
END
REACTIONS                                A          n    Ea,JOULES/MOLE
   O2+H=>OH+O                           2.00E+14  0.00  70300   ! 1
   OH+O=>O2+H                           1.46E+13  0.00   2080   ! 2
   H2+O=>OH+H                           5.06E+04  2.67  26300   ! 3
   OH+H=>H2+O                           2.24E+04  2.67  18400   ! 4
   H2+OH=>H2O+H                         1.00E+08  1.60  13800   ! 5
   H2O+H=>H2+OH                         4.45E+08  1.60  77130   ! 6
   OH+OH=>H2O+O                         1.50E+09  1.14    420   ! 7
   H2O+O=>OH+OH                         1.51E+10  1.14  71640   ! 8
   H+H+M=>H2+M                          1.80E+18 -1.00      0   ! 9
     O2/0.35/ H2O/6.5/ N2/0.5/
   H2+M=>H+H+M                          6.99E+18 -1.00 436080   ! 10
     O2/0.35/ H2O/6.5/ N2/0.5/
   H+OH+M=>H2O+M                        2.20E+22 -2.00      0   ! 11
     O2/0.35/ H2O/6.5/ N2/0.5/
   H2O+M=>H+OH+M                        3.80E+23 -2.00 499410   ! 12
     O2/0.35/ H2O/6.5/ N2/0.5/
   O+O+M=>O2+M                          2.90E+17 -1.00      0   ! 13
     O2/0.35/ H2O/6.5/ N2/0.5/
   O2+M=>O+O+M                          6.81E+18 -1.00 496410   ! 14
     O2/0.35/ H2O/6.5/ N2/0.5/
   H+O2+M=>HO2+M                        2.30E+18 -0.80      0   ! 15
     O2/0.35/ H2O/6.5/ N2/0.5/
   HO2+M=>H+O2+M                        3.26E+18 -0.80 195880   ! 16
     O2/0.35/ H2O/6.5/ N2/0.5/
   HO2+H=>OH+OH                         1.50E+14  0.00   4200   ! 17
   OH+OH=>HO2+H                         1.33E+13  0.00 168300   ! 18
   HO2+H=>H2+O2                         2.50E+13  0.00   2900   ! 19
   H2+O2=>HO2+H                         6.84E+13  0.00 243100   ! 20
   HO2+H=>H2O+O                         3.00E+13  0.00   7200   ! 21
   H2O+O=>HO2+H                         2.67E+13  0.00 242520   ! 22
   HO2+O=>OH+O2                         1.80E+13  0.00  -1700   ! 23
   OH+O2=>HO2+O                         2.18E+13  0.00 230610   ! 24
   HO2+OH=>H2O+O2                       6.00E+13  0.00      0   ! 25
   H2O+O2=>HO2+OH                       7.31E+14  0.00 303530   ! 26
   HO2+HO2=>H2O2+O2                     2.50E+11  0.00  -5200   ! 27
   OH+OH+M=>H2O2+M                      3.25E+22 -2.00      0   ! 28
     O2/0.35/ H2O/6.5/ N2/0.5/
   H2O2+M=>OH+OH+M                      2.10E+24 -2.00 206800   ! 29
     O2/0.35/ H2O/6.5/ N2/0.5/
   H2O2+H=>H2+HO2                       1.70E+12  0.00  15700   ! 30
   H2+HO2=>H2O2+H                       1.15E+12  0.00  80880   ! 31
   H2O2+H=>H2O+OH                       1.00E+13  0.00  15000   ! 32
   H2O+OH=>H2O2+H                       2.67E+12  0.00 307510   ! 33
   H2O2+O=>OH+HO2                       2.80E+13  0.00  26800   ! 34
   OH+HO2=>H2O2+O                       8.40E+12  0.00  84090   ! 35
   H2O2+OH=>H2O+HO2                     5.40E+12  0.00   4200   ! 36
   H2O+HO2=>H2O2+OH                     1.63E+13  0.00 132710   ! 37

END
```